

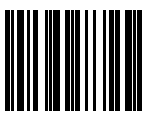
**Министерство науки и высшего образования Российской Федерации
ФЕДЕРАЛЬНОЕ ГОСУДАРСТВЕННОЕ АВТОНОМНОЕ ОБРАЗОВАТЕЛЬНОЕ
УЧРЕЖДЕНИЕ ВЫСШЕГО ОБРАЗОВАНИЯ
НАЦИОНАЛЬНЫЙ ИССЛЕДОВАТЕЛЬСКИЙ УНИВЕРСИТЕТ ИТМО
ITMO University**

**ВЫПУСКНАЯ КВАЛИФИКАЦИОННАЯ РАБОТА
GRADUATION THESIS**

Управление добротностью коллективных мод в цепочках связанных диэлектрических резонаторов / Engineering of High-Q Band-edge Modes in Chains of Coupled Dielectric Resonators

Обучающийся / Student Михайловский Михаил Сергеевич
Факультет/институт/кластер/ Faculty/Institute/Cluster физический факультет
Группа/Group Z42401
Направление подготовки/ Subject area 16.04.01 Техническая физика
Образовательная программа / Educational program Нанопотоника и метаматериалы 2020
Язык реализации ОП / Language of the educational program Английский
Статус ОП / Status of educational program МОП
Квалификация/ Degree level Магистр
Руководитель ВКР/ Thesis supervisor Савельев Роман Сергеевич, кандидат физико-математических наук, Университет ИТМО, физический факультет, старший научный сотрудник

Обучающийся/Student

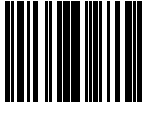
Документ подписан	
Михайловский Михаил Сергеевич	
07.06.2022	

(эл. подпись/ signature)

Михайловский
Михаил
Сергеевич

(Фамилия И.О./ name
and surname)

Руководитель ВКР/
Thesis supervisor

Документ подписан	
Савельев Роман Сергеевич	
07.06.2022	

(эл. подпись/ signature)

Савельев Роман
Сергеевич

(Фамилия И.О./ name
and surname)

**Министерство науки и высшего образования Российской Федерации
ФЕДЕРАЛЬНОЕ ГОСУДАРСТВЕННОЕ АВТОНОМНОЕ ОБРАЗОВАТЕЛЬНОЕ
УЧРЕЖДЕНИЕ ВЫСШЕГО ОБРАЗОВАНИЯ
НАЦИОНАЛЬНЫЙ ИССЛЕДОВАТЕЛЬСКИЙ УНИВЕРСИТЕТ ИТМО
ITMO University**

**ЗАДАНИЕ НА ВЫПУСКНУЮ КВАЛИФИКАЦИОННУЮ РАБОТУ /
OBJECTIVES FOR A GRADUATION THESIS**

Обучающийся / Student Михайловский Михаил Сергеевич

Факультет/институт/кластер/ Faculty/Institute/Cluster физический факультет

Группа/Group Z42401

Направление подготовки/ Subject area 16.04.01 Техническая физика

Образовательная программа / Educational program Нанوفотоника и метаматериалы
2020

Язык реализации ОП / Language of the educational program Английский

Статус ОП / Status of educational program МОП

Квалификация/ Degree level Магистр

Тема ВКР/ Thesis topic Управление добротностью коллективных мод в цепочках связанных диэлектрических резонаторов / Engineering of high-Q band-edge modes in chains of coupled dielectric resonators

Руководитель ВКР/ Thesis supervisor Савельев Роман Сергеевич, кандидат физико-математических наук, Университет ИТМО, физический факультет, старший научный сотрудник

Основные вопросы, подлежащие разработке / Key issues to be analyzed

Техническое задание / Thesis requirements:

Разработать экспериментально осуществимый дизайн резонансной структуры, поддерживающей высокодобротные коллективные моды. / To develop an experimentally feasible design of a resonant structure that supports high-Q band-edge modes.

Содержание работы / Contents:

1. Литературный обзор по тематике выпускной квалификационной работы.
2. Численное моделирование дисперсионных зависимостей бесконечных цепочек керамических резонаторов в микроволновом диапазоне спектра, с целью определения значений периода, при которых дисперсионные кривые становятся немонотонными вблизи края зоны Бриллюэна.
3. Численное моделирование конечных цепочек, состоящих из различного числа керамических резонаторов, с целью поиска высокодобротной моды, возникающей за счет взаимодействия коллективных мод через излучение континуума.
4. Численный расчёт зависимости добротности коллективной моды от числа резонаторов с учетом материальных потерь в керамике.
5. Численный расчёт экспериментально измеряемых параметров (параметров рассеяния) при возбуждении резонансов в цепочке при помощи электрической или магнитной дипольной антенны, расположенной с одного из концов цепочки. /

1. Literature review on the topic of the thesis.

2. Numerical calculation of the dispersion diagrams of infinite chains of ceramic resonators in the microwave range, in order to determine the period values at which the dispersion curves become nonmonotonic near the Brillouin zone edge.
3. Numerical calculation of finite chains consisting of different numbers of resonators, in order to find a high-Q mode resulting from the interaction of collective modes through the radiation continuum.
4. Numerical calculation of the dependence of the quality factor of the collective mode on the number of resonators, considering the material losses in ceramics.
5. Numerical calculation of experimentally measurable parameters (scattering parameters) when excitation of resonances in a chain by an electric or magnetic dipole antenna located at one end of the chain.

Рекомендуемые материалы и пособия для выполнения работы / Recommended materials and sourcebooks for completion of thesis:

1. Figotin A., Vitebskiy I., Slow wave phenomena in photonic crystals, Laser & Photonics Reviews, 5 (2), 201-213, 2011
2. Ding L. et al., All-optical modulation in chains of silicon nanoantennas, ACS Photonics, 7 (4), 1001-1008, 2020
3. Rutckaia V. et al., Coupling of Germanium Quantum Dots with Collective Sub-radiant Modes of Silicon Nanopillar Arrays, ACS Photonics, 8 (1), 209-217, 2020
4. Hoang T. X. et al., Collective Mie resonances for directional on-chip nanolasers, Nano Letters, 20 (8), 5655-5661, 2020
5. Kornovan D. F. et al., High-Q localized states in finite arrays of subwavelength resonators, ACS Photonics, 8 (12), 123627-3632, 2021

Дата выдачи задания / Assignment issued on: 15.01.2022

Срок представления готовой ВКР / Deadline for final edition of the thesis 20.05.2022

Характеристика темы ВКР / Description of thesis subject (topic)

Тема в области фундаментальных исследований / Subject of fundamental research: да / yes

СОГЛАСОВАНО / AGREED:

Руководитель ВКР/
Thesis supervisor

Документ подписан	
Савельев Роман Сергеевич	
31.03.2022	

(эл. подпись)

Савельев Роман
Сергеевич

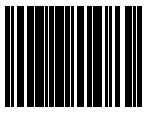
Задание принял к
исполнению/ Objectives
assumed BY

Документ подписан	
Михайловский Михаил Сергеевич	
31.03.2022	

(эл. подпись)

Михайловский
Михаил
Сергеевич

Руководитель ОП/ Head
of educational program

Документ подписан	
Богданов Андрей Андреевич	
15.04.2022	

Богданов
Андрей
Андреевич

(эл. подпись)

**Министерство науки и высшего образования Российской Федерации
ФЕДЕРАЛЬНОЕ ГОСУДАРСТВЕННОЕ АВТОНОМНОЕ ОБРАЗОВАТЕЛЬНОЕ
УЧРЕЖДЕНИЕ ВЫСШЕГО ОБРАЗОВАНИЯ
НАЦИОНАЛЬНЫЙ ИССЛЕДОВАТЕЛЬСКИЙ УНИВЕРСИТЕТ ИТМО
ITMO University**

**АННОТАЦИЯ
ВЫПУСКНОЙ КВАЛИФИКАЦИОННОЙ РАБОТЫ
SUMMARY OF A GRADUATION THESIS**

Обучающийся / Student Михайловский Михаил Сергеевич

Факультет/институт/кластер/ Faculty/Institute/Cluster физический факультет

Группа/Group Z42401

Направление подготовки/ Subject area 16.04.01 Техническая физика

Образовательная программа / Educational program Нанопотоника и метаматериалы
2020

Язык реализации ОП / Language of the educational program Английский

Статус ОП / Status of educational program МОП

Квалификация/ Degree level Магистр

Тема ВКР/ Thesis topic Управление добротностью коллективных мод в цепочках связанных диэлектрических резонаторов / Engineering of High-Q Band-edge Modes in Chains of Coupled Dielectric Resonators

Руководитель ВКР/ Thesis supervisor Савельев Роман Сергеевич, кандидат физико-математических наук, Университет ИТМО, физический факультет, старший научный сотрудник

**ХАРАКТЕРИСТИКА ВЫПУСКНОЙ КВАЛИФИКАЦИОННОЙ РАБОТЫ
DESCRIPTION OF THE GRADUATION THESIS**

Цель исследования / Research goal

Разработать экспериментально осуществимый дизайн резонансной структуры, поддерживающей высокодобротные коллективные моды. / To develop an experimentally feasible design of a resonant structure that supports high-Q band-edge modes.

Задачи, решаемые в ВКР / Research tasks

1. Численное моделирование дисперсионных зависимостей бесконечных цепочек диэлектрических резонаторов, с целью определения значений периода, при которых дисперсионные кривые становятся немонотонными вблизи края зоны Бриллюэна. 2. Численное моделирование конечных цепочек, состоящих из различного числа диэлектрических резонаторов, с целью поиска высокодобротной моды, возникающей за счет взаимодействия коллективных мод через радиационный континуум. 3. Численный расчёт зависимости добротности коллективной моды от числа резонаторов, для цепочки керамических резонаторов учитывается влияния материальных потерь, для случая оптической резонансной цепочки учитывается влияния подложки. 4. Численный расчёт экспериментально измеряемых параметров (параметров рассеяния) для цепочки керамических резонаторов при возбуждении резонансов в цепочке при помощи электрической или магнитной дипольной антенны. 5. Анализ влияния вариаций геометрических и материальных параметров на рассматриваемый эффект. / 1. Numerical

calculation of the dispersion diagrams of infinite chains of dielectric resonators, in order to determine the period values at which the dispersion curves become nonmonotonic near the Brillouin zone edge. 2. Numerical calculation of finite chains consisting of different numbers of resonators, in order to find a high-Q mode resulting from the interaction of collective modes through the radiation continuum. 3. Numerical calculation of the dependence of the quality factor of the collective mode on the number of resonators, for a chain of ceramic resonators the effect of material losses is taken into account, for the case of an optical resonant chain the influence of the substrate is taken into account. 4. Numerical calculation of experimentally measurable parameters (scattering parameters) for a chain of ceramic resonators at excitation of resonances in a chain by an electric or magnetic dipole antenna. 5. Analysis of the influence of variations in geometric and material parameters on the considered effect.

Краткая характеристика полученных результатов / Short summary of results/findings

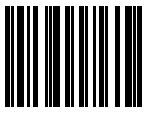
В данной работе исследовалась возможность экспериментальной реализации цепочки диэлектрических резонаторов, поддерживающей высокودобротные моды, которые возникают из-за взаимодействия двух коллективных мод цепочки через радиационный континуум. Было проанализировано, какие геометрические и материальные параметры позволяют достичь такого режима. Исследовано, как влияют на рассматриваемый эффект существующие каналы потерь, а именно материальные потери и дополнительное рассеяние, вызванное вариацией геометрических и материальных параметров. На основе проведённого анализа разработаны две возможные конфигурации цепочек керамических резонаторов, поддерживающие высокودобротные коллективные моды в микроволновом спектральном диапазоне. Проведены экспериментальные измерения спектрального отклика предложенных структур, подтверждающие основные предсказанные результаты. Также теоретически были рассмотрены реалистичные конфигурации наноструктур, поддерживающие высокودобротные коллективные моды в оптическом спектральном диапазоне. Показано, что предсказанный эффект является достаточно общим и может наблюдаться для цепочек резонаторов с модами разного типа. В качестве примера разработана конфигурация, поддерживающая высокودобротные коллективные моды с доминирующими магнитным дипольным и магнитным квадрупольным моментами. Добротность магнитной квадрупольной моды превышала добротность моды дипольного типа примерно на порядок и допускала большее отклонения значения периода от оптимального, что может являться преимуществом для будущих оптических экспериментов. / In this work, we have investigated the possibility of experimental realization of the chain of dielectric resonators that support eigenmodes with high quality factors that appear due to interaction of two collective modes of the chain via radiation continuum. We have analyzed what kind of geometrical and material parameters allow to achieve such regime. We have investigated how the present channels of losses, namely material losses and additional scattering due to variation in geometrical and materials parameters, influence the considered effect. Based on the performed analysis we have developed two feasible designs of the chains of ceramic resonators, that support high-Q modes in microwave spectral range. We have performed experimental measurements of the spectral response of the proposed structures which confirmed the main predicted results. We have also theoretically considered realistic nanostructures supporting high-Q band-edge modes in optical frequency range. We have shown that the predicted effect is quite general and can be observed for the mode of the resonator chain of any type. As an example, we have developed a design that supports modes with dominant magnetic dipole and magnetic quadrupole moments excited in the nanoparticles. The Q-factor of the magnetic quadrupole mode exceeded that of the dipole-type mode by approximately 1 order and allowed for larger deviation of the value of the period from the optimal one, which can be advantageous for the future optical experiments.

Наличие выступлений на конференциях по теме выпускной работы / Conference

reports on the topic of the thesis

1. Школа-конференция с международным участием по оптоэлектронике, фотонике и нанобиоструктурам Saint Petersburg OPEN 2022, 24.05.2022 - 27.05.2022 (Конференция, статус - международный)

Обучающийся/Student

Документ подписан	
Михайловский Михаил Сергеевич	
07.06.2022	

(эл. подпись/ signature)

Михайловский
Михаил
Сергеевич

(Фамилия И.О./ name
and surname)

Руководитель ВКР/
Thesis supervisor

Документ подписан	
Савельев Роман Сергеевич	
07.06.2022	

(эл. подпись/ signature)

Савельев Роман
Сергеевич

(Фамилия И.О./ name
and surname)

CONTENTS

ABBREVIATIONS	9
INTRODUCTION	10
1 LITERATURE REVIEW AND METHODS.....	12
1.1 Literature review	12
1.2 Theoretical introduction	17
1.3 Methods	21
Conclusions on Chapter 1	27
2 CHAIN OF COUPLED CERAMIC RESONATORS.....	28
2.1 Analysis of the material and geometrical parameters required for experimental observation	28
2.2 Results of numerical simulations	29
2.3 Experimental verification	35
2.4 Chain of ceramic cylinders in coaxial arrangement	39
Conclusions on Chapter 2	44
3 CHAIN OF COUPLED SILICON RESONATORS	45
3.1 Results of numerical simulations	46
Conclusions on Chapter 3	48
CONCLUSION	51
REFERENCES	52

ABBREVIATIONS

MD – Magnetic dipole

ED – Electric dipole

MQ – Magnetic quadrupole

EQ – Electric quadrupole

PEC – Perfect electric conductor

PMC – Perfect magnetic conductor

PMLs – Perfectly matched layers

WGM – Whispering gallery mode

PhC – Photonic crystal

MPs – Micropillars

BE – Band-edge

DBE – Degenerate band-edge

INTRODUCTION

All-dielectric optical resonant structures supporting resonances with high quality factors and allowing to localize electromagnetic fields in a small volume are of both fundamental and applied interest due to significant increase of light-matter interaction strength. One type of such structures are ensembles of coupled dielectric subwavelength resonators [1, 2]. Due to the interference of radiation from individual elements, such structures support collective resonant oscillations, characterized by suppressed radiative losses and consequently high quality factors. It has been experimentally shown that such systems allow to enhance the nonlinear response of the material of which they are made [2], to enhance the photoluminescence intensity of the quantum dots integrated into them [3], and to achieve regime of laser generation [4]. Besides destructive interference between radiation from individual resonators in an ensemble, coupling between two or more modes via radiation continuum can occur under variation of the parameters of such structures. In this case the quality factor of one of the eigenmodes can be substantially increased. For example, this can be achieved by precision control of the gap between individual resonators in the chain [5]. This mechanism can be explained by a change of the dispersion curve of the corresponding infinite chain of resonators, namely, by the appearance of an inflection point near the edge of the Brillouin zone, which leads to the destructive mode interference of the corresponding finite chain. However, this effect has been predicted only theoretically and not investigated experimentally.

In this work, we have investigated the possibility of experimental realization of the chain of dielectric resonators that support eigenmodes with high quality factors that appear due to interaction of two collective modes of the chain via radiation continuum. We have analyzed what kind of geometrical and material parameters allow to achieve such regime. We have investigated how the present channels of losses, namely material losses and additional scattering due to variation in geometrical and materials parameters, affect the considered effect. Based on the performed analysis we have developed two feasible designs of the chains of ceramic resonators, that support high- Q modes in microwave spectral range. We have performed experimental measurements of the spectral response of the proposed structures which confirmed the main predicted results. We have also theoretically considered realistic nanostructures supporting high- Q band-edge modes

in optical frequency range. We have shown that the predicted effect is quite general and can be observed for the mode of the resonator chain of any type. As an example, we have developed a design that supports modes with dominant magnetic dipole and magnetic quadrupole moments excited in the nanoresonators. The Q -factor of the magnetic quadrupole mode exceeded that of the dipole-type mode by approximately 1 order and allowed for larger deviation of the value of the period from the optimal one, which can be advantageous for the future optical experiments.

1 LITERATURE REVIEW AND METHODS

1.1 Literature review

Efficient manipulation of optical radiation at the nanoscale is the main goal of nanophotonics. Conventionally, optical resonant structures are employed for this purpose since they allow for enhancement of the light-matter interaction required for generation and processing of optical signals in optical and optoelectronic devices. For example, the operation of any of such devices requires active components, or the sources of the signal, which in turn will be connected to many other parts of the device by passive interconnections. This is achieved by integration of active media, such as quantum dots, solid-stated defects, 2D materials etc. with different kinds of specially designed optical resonators, which can make the emission from these quantum source more efficient and flexible. Therefore, the development of new designs and improvement of the current designs of optical resonators is one of the constantly developing subjects in the area of nanophotonics.

One of the key characteristics that determines the enhancement of light-matter interaction in optical resonators is the coupling strength between the quantum source and the particular mode of the optical structure, determined by the Q/V_{mode} ratio, where Q is the quality factor, and V_{mode} is the mode volume. Such characteristic, however, describes the coupling strength only for a single point-like emitter located at the antinode of the resonator eigenmode. In certain situations the very strong localization of the field is not so beneficial, since the coupling between many distributed sources within the resonator is required. The quality factor itself also can not be considered as the universal figure-of-merit, since there is always an upper limit on the desired Q due spectral width of the optical signal. Another characteristic, which can be important is the geometrical size of the resonator. Small size of the resonator can allow for reducing of the footprint of devices as well as e.g. reducing the heat absorption. In order to create a picture of the variety of current designs of optical resonators, we have classified the main types and designs from the literature based on the values of these characteristics, which for illustrative purposes is shown in Fig. 1.

While in some cases conversion of optical energy into heat can put a constraint on the maximal possible value of the Q -factor of a cavity, there are various dielectric materials in the optical frequency range, for which Ohmic losses can be neglected. The radiative losses, on the other hand, are inevitable due to the na-

ture of photons, which unlike electrons cannot exist in purely bound states in any realistic finite-size optical structure. However, there is no limit on how small the radiative losses can be, and suppressing of this loss channel by means of different mechanisms and different designs of photonic nanostructures has gained a lot of interest during last decades.

One possible design of optical resonators are disk, ring, and toroidal resonators supporting WGM resonant modes. Such resonators are of great interest for applications in optical and optoelectronic devices [6], as well as in fundamental cavity quantum electrodynamics research [7]. A characteristic feature of optical WGM resonators is the record high values of the achieved quality factors, however, for relatively large structures. For a silica toroidal microcavity, with the the outer and inner diameters of $29 \mu\text{m}$ and $6 \mu\text{m}$, respectively, the quality factor $Q \approx 4 \times 10^8$, mode volume $V_{\text{mode}} \approx 180 \mu\text{m}^3$ for a resonant wavelength of $\lambda = 1550 \text{ nm}$, with the corresponding ratio $Q/V_{\text{mode}} \approx 2.5 \times 10^6 (\lambda/n)^{-3}$ were obtained experimentally [8]. In [9] a chip-integrated disk microresonator with a radius of $3.5 \mu\text{m}$ and a thickness of 160 nm , fabricated of GaAs and optically coupled to adjacent single-mode waveguides. The intrinsic quality factor of the resonator $Q \approx 2.3 \times 10^4$ with the corresponding mode volume $V_{\text{mode}} \approx 18 (\lambda/n)^3$ near the $\lambda \approx 930 \text{ nm}$ were achieved. Then for this structure we estimate $Q/V_{\text{mode}} \approx 1270 (\lambda/n)^{-3}$.

Another class of optical resonators are PhC cavities. The advantages of such a platform include their ability to be easily integrated on a chip. In the paper [10], for silicon PhC microcavity, were experimentally obtained $Q \approx 2 \times 10^6$, with $V_{\text{mode}} \approx 0.96 (\lambda/n)^3$ for the corresponding resonant wavelength $\lambda = 1550 \mu\text{m}$ which gives an estimate of $Q/V_{\text{mode}} \approx 2 \times 10^6 (\lambda/n)^{-3}$, are of the same order of magnitude as the values obtained for the ultra-high- Q WGM resonators, but at the same time having a much smaller mode volume. Also a possible PhC design is a one-dimensional structure, with a set of holes in a high-index material, to create a periodic change in refractive index, called a PhC nanobeam cavity. In such structures, the mode is strongly localized in the defective region, which is created by modulating the distance at which the individual holes are located in the central region of the structure. In [11], for the considered GaAs nanobeam structure, with a length of the order of several micrometers, a thickness of 130 nm and a width of 370 nm , obtained $Q \approx 25000$, $V_{\text{mode}} \approx 0.38 (\lambda/n)^3$ for the resonant

wavelength of 945 nm, therefore, $Q/V_{\text{mode}} \approx 6.58 \times 10^4 (\lambda/n)^{-3}$. Also, PhC resonators can represent micropillars (MPs) consisting of a set of periodic layers with distributed Bragg reflectors at the top and bottom of the structure. In [12], for MP resonators with a diameter of about 1 μm and a height of about 10 μm , fabricated of GaAs/AlAs layers the experimentally obtained characteristics was $Q \approx 13600$, $V_{\text{mode}} \approx 2.3 (\lambda/n)^3$ for $\lambda = 950$ nm, therefore, $Q/V_{\text{mode}} \approx 5900 (\lambda/n)^{-3}$.

Record low mode volume values can be obtained using metallic structures supporting localized surface plasmon resonances (LSPR), collective oscillations of free electrons occurring in metallic structures excited by light with the corresponding wavelength. In such structures it is possible to achieve almost any small region in which a mode will be localized, limited almost by the precision of the sample fabrication methods. However, the requirement to use metallic structures is a very limiting factor for the maximum possible quality factor for such structures because of the strong losses in the optical range. In [13], for a dimer structure composed of aluminum nanoantennas with sides of the order of 100 nm, it was possible to localize the mode in the 10 nm gap between the antennas, with the corresponding $Q \approx 6$, $V_{\text{mode}} \approx 2 \times 10^{-3} (\lambda/n)^3$. Then we can estimate $Q/V_{\text{mode}} \approx 3000 (\lambda/n)^{-3}$. Experimentally also realized structures representing PhC nanobeam cavity, located on a metallic substrate. This design of a hybrid structure allows to achieve localization of the mode in a very small area, while significantly increasing the quality factor, compared to other plasmonic structures. In [14], lasing was experimentally demonstrated for a structure representing a nanobeam waveguide fabricated of a semiconductor heterostructure InGaAsP/InP placed on a gold substrate, demonstrating $Q \approx 180$ and $V_{\text{mode}} \approx 0.3 (\lambda/n)^3$.

In this work, we study the resonators based on the periodic structures that support the so-called band edge states or collective eigenmodes. Such regular collective resonances in a finite slab of a periodic structure represent a standing wave with a characteristic wave number near the edge of the Brillouin zone of the corresponding infinite structure. The quality factor of such resonances can be relatively high due to the low group velocity of the waves, and as the size of the structure tends to infinity, the inverse group velocity diverges, which is known as the optical analog of the Van Hove singularity. One of the simplest systems in which such an effect was observed is periodic layered structures [15, 16]. In the context of nanophotonics and nanocavities, such an effect was theoretically predicted

and confirmed experimentally in the microwave frequency range for an array of dielectric particles supporting magnetic dipole resonance [17]. Later, this effect was used in several theoretical and experimental works to enhance luminescence, enhance nonlinear effects, and create a nanolaser [2–4, 18]. In [2], the presence of propagating modes in a chain of silicon nanoresonators with a low group velocity of the order of $c/100$, was experimentally demonstrated. The fabricated chain of nanoresonators was integrated with the waveguide, and thus the authors could measure the transmission coefficients of the optical signal, demonstrating the values of $Q \approx 1.38 \times 10^4$ and $V_{\text{mode}} \approx 2.55 (\lambda/n)^3$ with the corresponding $Q/V_{\text{mode}} \approx 5400 (\lambda/n)^{-3}$. In [18], the same group of authors studied a similar geometry – a chain of nanoresonators (30-60 particles) integrated with a homogeneous waveguide in the end-fire configuration. The structure parameters were optimized for the employed lithographic methods and for the maximization of the Q -factor of the chain modes, which reached values up to 14000. Using this structure, the authors demonstrated the possibility of its functioning as a modulator integrated into optical chips, and controlled by excitation of free carriers in silicon by external radiation, with a characteristic response time of 50 ps and switching energy of 50 fJ. It should be noted that some of the structures were fabricated by optical lithography compatible with CMOS technologies. In [4], the authors of the same group demonstrated lasing in an array of nanoresonators. This time, the particles were made from a direct-gap semiconductor, gallium arsenide, and the array of nanoresonators was not integrated with the waveguide. Despite the rather large size of the structure – 100 nanoresonators (about 25 wavelengths in the longitudinal direction) – the quality factor of the resonance was only 1000. However, even this quality factor was enough to achieve the lasing regime. It is worth noting that because of the above-mentioned directivity patterns of collective modes (along the axis of the chain), only a very small fraction of emission can be straight-forwardly collected in the far field from the top, therefore, schemes relied on the coupling of such structures with the optical homogeneous waveguides look preferable. In [3], the enhancement of luminescence from germanium quantum dots grown in silicon due to the interaction with the collective modes of an array of silicon nanopillars was experimentally shown. In particular, it has been shown that a simple one-dimensional array supports various types of resonances that can be used to enhance the emission. The obtained quality factor value was about

500, with the corresponding mode volume of $3 (\lambda/n)^3$. Despite the low values of the quality factors compared with, for example, one-dimensional photonic-crystal resonators of the “nanobeam” type, the enhancement of the luminescence intensity reached values of the order of 10.

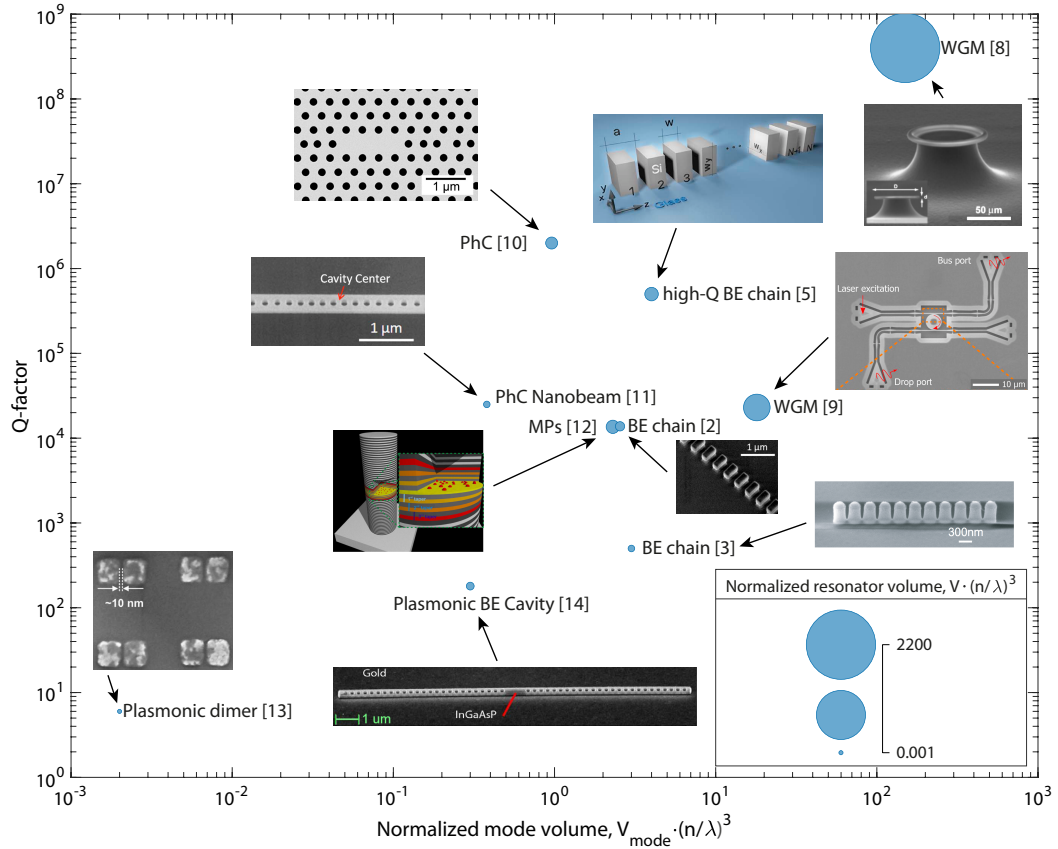


Figure 1 – Characteristics of nano- and microresonators for visible and near-IR spectral range. The references specified in square brackets correspond to the numbering of the references in this work.

The possibility of a significant increase in the quality factor of such modes due to the interaction of the modes via radiation continuum [19] was considered only in a few works [5, 20–23]. In the case of a one-dimensional array, such an effect was demonstrated in the context of cold atoms in free space and integrated with a waveguide [21, 22], as well as for a one-dimensional array of silicon nanoresonators [5], in which the quality factor for small structures with a size of about 2-3 wavelengths per longitudinal direction was 1-6 thousands, which is comparable with photonic-crystal resonators of the same size [23], and the mode volume of about 1-4 $(\lambda/n)^3$. It should be noted that when using the such effect of Q -factor boost, it is possible to achieve a significantly faster growth rate of the Q -factor

with the size of the array (up to N^7 for a one-dimensional array [5], where N is the number of periods in the structure). In this case, despite the fact that photonic crystal resonators or whispering gallery resonators allow for an exponential increase in the quality factor with size, this is achieved either through the use of an adiabatic taper that complicates the fabrication procedure, and/or is achieved only at sufficiently large sizes of tens of microns [23]. At small sizes, they become comparable in quality factor with collective resonances or even smaller.

However, this effect of the quality factor boost, firstly, has not been experimentally demonstrated up to date, secondly, the effect of material losses and variation in the parameters of the system has not been considered, and third, the analysis of what kind of geometrical and material parameters, e.g. shape of the particles could be feasible for experimental realization. These problems will be the focus of the current work.

1.2 Theoretical introduction

The most well-known example of an optical structure that can trap light for many oscillation periods is the Fabry–Pérot resonator, which in its simplest form presents two plane mirrors filled with a transparent dielectric material. The only factor that prevents the light from getting out of such cavity is the high reflection coefficient (close to unity) of the mirrors.

Let us, first, recall the origin of the power dependence of the quality factor on the length L of the Fabry-Pérot resonator for such conventional type of the cavity, schematically shown in Figure 2(a). The modes of a finite cavity represent a standing wave, typically formed by the two counter-propagating plane waves with wavenumbers k that satisfy the boundary conditions. The real part of the eigenfrequencies of such resonances can be quite accurately estimated from the dispersion of the infinite system, which is linear if the system is filled with transparent dielectric material. The imaginary part or the quality factor of the resonance then depends on three factors: first, the group velocity of the propagating waves at the resonance frequency v_g , second, the length of the cavity, and third, the reflection coefficient at the boundary between the inner material and semi-infinite cladding layers r . The time spent by the photon in the cavity is $\tau \propto L/v_g$, while the fraction of energy lost after each pass is proportional to $(1 - |r|^2)$. Therefore, Q -factor of

the resonance is determined as follows:

$$Q \propto \frac{L}{v_g(1 - |r|^2)}. \quad (1)$$

In the case of conventional Fabry-Pérot cavity the group velocity is constant and does not depend neither on the frequency, nor on the length of the cavity. The same is true for the reflection coefficient. Consequently, the Q -factor linearly depends on the length of the cavity.

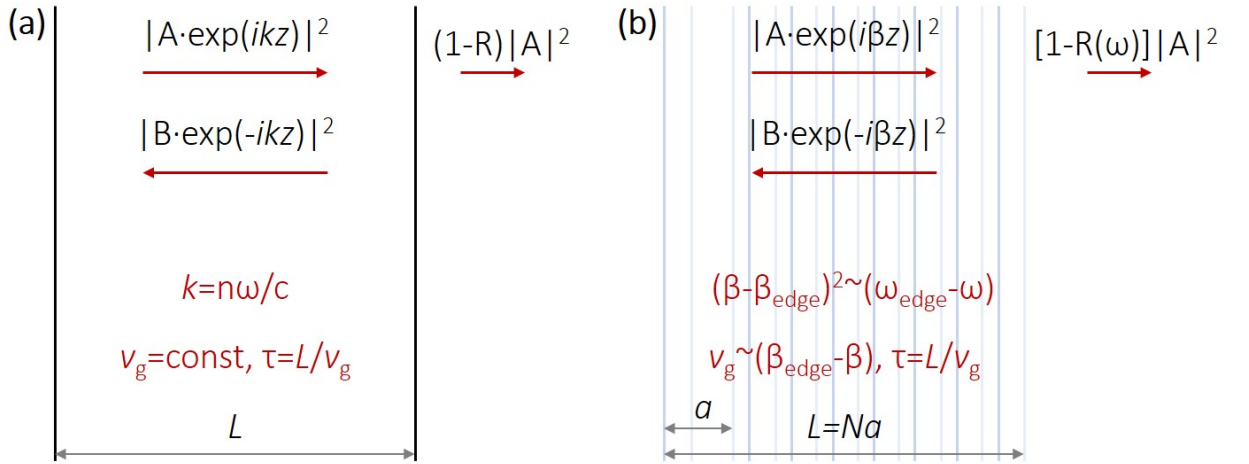


Figure 2 – Schematic of the (a) conventional Fabry-Pérot cavity filled with homogeneous dielectric material and (b) slab of the PhC layered structure.

The development of photonic crystals (PhC) led to the idea of filling the space between the mirrors with a periodic layered structure, as schematically shown in Figure 2(b). In this case the mirrors on the sides are actually not needed, due to high reflection coefficient between homogeneous dielectric and PhC at frequencies close to the edge of the PhC band gap [24]. We can apply the same reasoning for the slab of the PhC as for the conventional Fabry-Pérot cavity.

In the case of the layered structure the modes of a finite periodical system represent a standing wave formed by the two counter-propagating Bloch modes with Bloch wavenumbers β that satisfy the boundary conditions. Dispersion of the infinite system is now not linear but has a complicated behaviour in general [24]. We are mostly interested in the dispersion near the band gap (the edge of the Brillouin zone). Due to time-reversal symmetry the group velocity $v_g = d\omega/d\beta$ of PhC modes vanishes when the Bloch wavenumber reaches the edge of the Brillouin zone. The necessarily non-zero second derivative $d^2\omega/d\beta^2$ leads to the parabolic

dispersion and the linear dependence of group velocity on the Bloch wavenumber $v_g \propto \Delta\beta = (\pi/a - k)$, where a is the period of the structure.

Further, it can be shown that the reflection coefficient for frequencies close to the PhC band gap also linearly depends on $\Delta\beta$ [24]. When considering a finite-size system consisted of N periods, the wavenumber that corresponds to the resonance with the highest quality factor scales as $\beta_{\text{res}} = \pi/a(1 - 1/N)$ [25]. Now if we combine all these factors, we get the following dependence of the Q -factor on the number of the periods N (or the length of the structure):

$$Q \propto \frac{L}{v_g(1 - |r|^2)} \propto N^3. \quad (2)$$

Such behaviour is inherent to many periodic systems. The system that we consider in our work – a chain of dielectric particles also typically exhibits such behaviour [1].

Recently, it was suggested that the mixture of two modes in specially designed periodic structures, e.g. in a layered system made of anisotropic materials, can lead to the quartic dispersion near the edge of the Brillouin zone, unlike quadratic dispersion typically observed in periodic structures [25]. It was shown that this so-called degenerate-band-edge (DBE) regime can be realized in many types of one-dimensional systems, whenever the dispersion dependence $\Delta\omega \propto \Delta\beta^4$ is achieved. Again, applying the same arguments, one can conclude that as compared to the conventional periodic structure only the group velocity dependence on N changes to $v_g \propto 1/N^3$. Therefore, despite of the more complicated design and additional restrictions on the robustness of the operation, such modification leads to the much faster growth of the quality factor with the increase of the cavity size $Q \propto N^5$, which allows to substantially miniaturize the size of an optical resonator for a given value of the Q -factor. In general, if the dispersion dependence near the edge of the Brillouin zone is given by $\Delta\omega \propto \Delta k^s$, the $Q(N)$ dependence is given by $Q \propto N^{(s+1)}$. This was shown independently for the one-dimensional arrays of dipole scatterers [26], which allows to believe that such behaviour is general for any periodic structure.

In order to achieve a quartic dispersion for layered structures it is necessarily required to have two modes with different polarizations mixed in a specific way [27]. This approach is based on the combining two parabolic dispersion in a

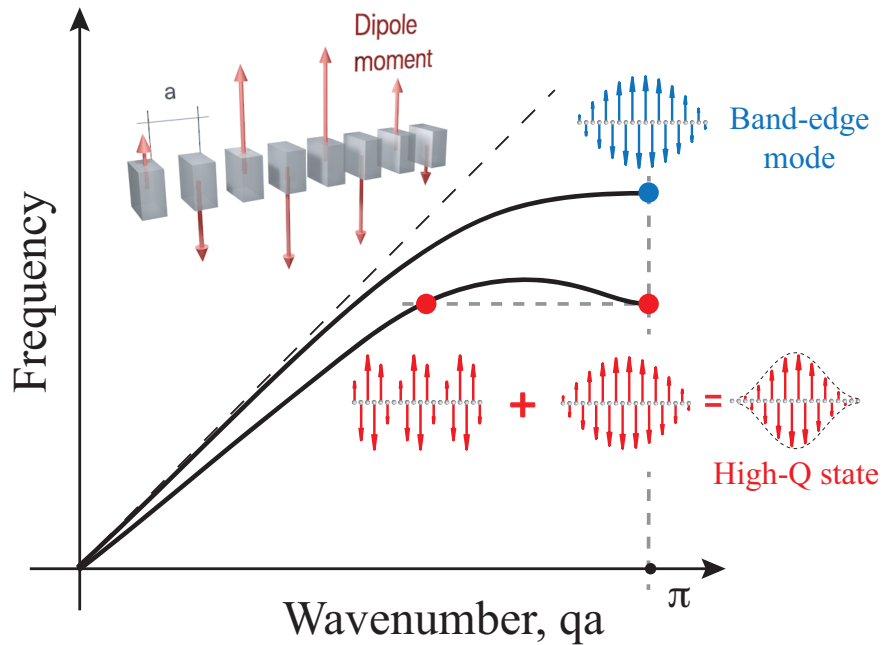


Figure 3 – An inflection point in the dispersion curve of an infinite one-dimensional array of dipole scatterers (an upper inset) enables interference between the staggered band-edge mode and another standing mode of a finite-extent array, thus suppressing radiative losses with the formation of a high- Q localized state. From the Ref. [5].

certain way, such that the group velocity dispersion cancels at the edge of the Brillouin zone. This was employed in the experiment with photonic crystal waveguides, where authors developed the structure with two coupled single-mode PhC waveguides [28]. By controlling the coupling between the waveguides they were able to achieve the quartic type of dispersion and show experimentally $Q \propto N^5$ dependence. For an arbitrary periodic structure, however, the dispersion relation can be quite complicated and the condition of zero second order dispersion can be satisfied even in a single mode regime. For example, it was shown that the chain of dipole scatterers exhibits quartic dispersion for a specific value of the period a_{DBE} that can be found analytically [5].

The more peculiar situation can be realized when the chosen parameter, e.g. the period of the chain a , exceeds the critical parameter a_{DBE} and the second order dispersion changes the sign at the edge of the Brillouine zone. The dispersion then becomes nonmonotonic and the dependence $Q(N)$ of the corresponding finite system also changes drastically. In this case the eigenmodes of the finite system can interact via radiation continuum due to relatively close real part of the frequencies [5]. This is schematically illustrated in Figure 3 borrowed from the Ref. [5],

where it was shown that the dependence of the Q -factor on the size of the chain of dipole scatterers becomes nonmonotonic exhibiting a maximum that exceeds the Q -factor for any other value of period by almost two orders for a considered system. In fact, by varying the period one can find the optimal one, i.e. for which the radiation losses substantially reduce for a given value of number of periods N , which allow to substantially reduce the size of resonators. The aim of the current work is to develop a design for the experimental realization of the structures that support such high- Q band edge states and to perform the measurement of their characteristics.

1.3 Methods

1.3.1 Multipole decomposition

To analyze resonant modes of a single resonator in a chain we have performed a multipole decomposition using the method proposed by [29, 30], which allows one to consider particles of arbitrary shape.

Consider an arbitrary shaped particle located at the origin of a Cartesian coordinate system. A plane monochromatic wave with the time dependence defined by $\exp(-i\omega t)$ is scattered on the particle, where ω is the angular frequency. The incident wave induces a polarization of the form $\mathbf{P} = \varepsilon_0(\varepsilon_p - \varepsilon_m)\mathbf{E}$, where ε_0 is the vacuum dielectric constant, ε_p is the relative dielectric permittivity of the particle, ε_m is the relative dielectric permittivity of the surrounding medium, \mathbf{E} is the total electric field inside the particle. We write the light-induced polarization as

$$\mathbf{P}(\mathbf{r}) = \int \mathbf{P}(\mathbf{r}')\delta(\mathbf{r} - \mathbf{r}') d\mathbf{r}', \quad (3)$$

and then expand the Dirac delta function $\delta(\mathbf{r} - \mathbf{r}')$ in a Taylor series around a point \mathbf{r}_0 we can write [29]:

$$\mathbf{P}(\mathbf{r}) \simeq \mathbf{p}\delta(\mathbf{r}) + \frac{i}{\omega}\nabla \times \mathbf{m}\delta(\mathbf{r}) - \frac{1}{6}\hat{Q}\nabla\delta(\mathbf{r}) - \frac{i}{2\omega}\nabla \times \hat{M}\nabla\delta(\mathbf{r}), \quad (4)$$

where

$$\mathbf{p} = \int \mathbf{P}(\mathbf{r}') d\mathbf{r}', \quad (5)$$

$$\mathbf{m} = -\frac{i\omega}{2} \int \mathbf{r}' \times \mathbf{P}(\mathbf{r}') d\mathbf{r}', \quad (6)$$

$$\hat{Q} = 3 \int (\mathbf{r}' \otimes \mathbf{P}(\mathbf{r}') + \mathbf{P}(\mathbf{r}') \otimes \mathbf{r}') d\mathbf{r}', \quad (7)$$

$$\hat{M} = -\frac{2i\omega}{3} \int (\mathbf{r}' \times \mathbf{P}(\mathbf{r}')) \otimes \mathbf{r}'' d\mathbf{r}', \quad (8)$$

are the electric dipole moment, the magnetic dipole moment, the electric quadrupole moment, and the magnetic quadrupole moment, respectively. Considering only these four multipoles, for the scattered field $\mathbf{E}_{\text{sc}}(\mathbf{r})$, we can write

$$\mathbf{E}_{\text{sc}}(\mathbf{r}) \simeq \frac{e^{ik_m r}}{r} \mathbf{E}_0^{\text{sc}}(\mathbf{n}), \quad (9)$$

where

$$\begin{aligned} \mathbf{E}_0^{\text{sc}}(\mathbf{n}) \simeq & \frac{k_0^2}{4\pi\epsilon_0} \left(\mathbf{n} \times (\mathbf{p} \times \mathbf{n}) + \frac{\sqrt{\epsilon_m}}{c} \mathbf{m} \times \mathbf{n} \right. \\ & \left. + \frac{ik_m}{6} \mathbf{n} \times (\mathbf{n} \times \hat{Q}\mathbf{n}) + \frac{i\sqrt{\epsilon_m}k_m}{2c} \mathbf{n} \times (\hat{M}\mathbf{n}) \right), \end{aligned} \quad (10)$$

is the scattering amplitude into the direction \mathbf{n} (\mathbf{n} is the unit vector directed along \mathbf{r}), k_0 is the wave number in vacuum, k_m is the wave number in the surrounding medium, c is the speed of light in vacuum. The far-field scattered power dP_{sc} into the solid angle $d\Omega = \sin\theta d\theta d\varphi$ is determined by the time-averaged Poynting vector

$$dP_{\text{sc}} = \frac{1}{2} \sqrt{\frac{\epsilon_0\epsilon_m}{\mu_0}} |\mathbf{E}_{\text{sc}}|^2 r^2 d\Omega, \quad (11)$$

where μ_0 is the vacuum permeability. Substituting Eq. (10) into Eq. (11) and integrating over the solid angle, we obtain the total scattering power

$$\begin{aligned} P_{\text{sc}} \simeq & \frac{\sqrt{\epsilon_m}k_0^4}{12\pi\epsilon_0^2\mu_0c} |\mathbf{p}|^2 + \frac{\epsilon_m^{3/2}k_0^4}{12\pi\epsilon_0c} |\mathbf{m}|^2 \\ & + \frac{\epsilon_m^{3/2}k_0^6}{1440\pi\epsilon_0^2\mu_0c} \sum_{\alpha\beta} |Q_{\alpha\beta}|^2 + \frac{\epsilon_m^{5/2}k_0^6}{160\pi\epsilon_0c} \sum_{\alpha\beta} |M_{\alpha\beta}|^2. \end{aligned} \quad (12)$$

The scattering cross section σ_{sc} is defined from P_{sc} by normalization to the energy flux of the incident wave $I_{\text{inc}} = 1/2\sqrt{(\epsilon_0\epsilon_m/\mu_0)}|\mathbf{E}_{\text{sc}}|^2$:

$$\sigma_{\text{sc}} \simeq \frac{k_0^4}{6\pi\epsilon_0^2|\mathbf{E}_{\text{inc}}|^2} |\mathbf{p}|^2 + \frac{\mu_0\epsilon_mk_0^4}{6\pi\epsilon_0|\mathbf{E}_{\text{inc}}|^2} |\mathbf{m}|^2$$

$$+ \frac{\varepsilon_m k_0^6}{720\pi\varepsilon_m^2 |\mathbf{E}_{\text{inc}}|^2} \sum_{\alpha\beta} |Q_{\alpha\beta}|^2 + \frac{\mu_0 \varepsilon_m^2 k_0^6}{80\pi\varepsilon_0 |\mathbf{E}_{\text{inc}}|^2} \sum_{\alpha\beta} |M_{\alpha\beta}|^2. \quad (13)$$

1.3.2 Numerical simulations

Numerical simulations of the characteristics of the chains of ceramic cylinders were done in COMSOL Multiphysics. The main characteristics that we wanted to obtain were dispersion proprieties (mostly below the light line) of the infinite chains and the eigenfrequencies and Q -factors of the finite chains of the cylinders. To study the properties of the infinite chains we have created a 3D model that included a domain with a single cylinder surrounded by vacuum (unit cell of an infinite periodic chain). In the direction of the translational symmetry the size of the domain was equal to the period of the chain a , with corresponding periodic Floquet boundary conditions that allowed for variation of the Bloch wavenumber. In the other two directions we employed two options for the boundary conditions. In the first one the computational domain consisted only of the background layer and on the transverse boundaries the perfect electric or magnetic conductors were imposed. In this way for large enough background distance (approximately $\lambda/4$) we were able to find the waveguide modes (below the light line) of the chain with zero material losses. Mostly, this was enough to understand the general behaviour of the dispersion and to provide expectations for the finite chains. For the sake of completeness we have also solved the more general problem that allows to find all modes including radiative modes above the light line and to take into account material losses in the resonators. To calculate dispersion curves, scattering boundary conditions can be used as open boundary conditions. This gives a sufficient level of accuracy and at the same time reduces the computational domain, which also reduces the computational time. A schematic representation of the computational domain for calculating dispersion dependencies is shown in Fig. 4. PEC and PMC boundaries are chosen based on the symmetry of the mode of interest. For the PEC boundary conditions we have $\mathbf{n} \times \mathbf{E} = 0$, where \mathbf{n} is the unit normal vector, \mathbf{E} is the electric field, i.e. the tangential components of the electric field at the boundary are zero. And for the PMC boundary conditions we have $\mathbf{n} \times \mathbf{H} = 0$, where \mathbf{H} is the magnetic field, i.e. the tangential component of the magnetic field at the boundary are zero. In order to obtain a complete mode structure in one calculation it is necessary not to use the symmetry planes.

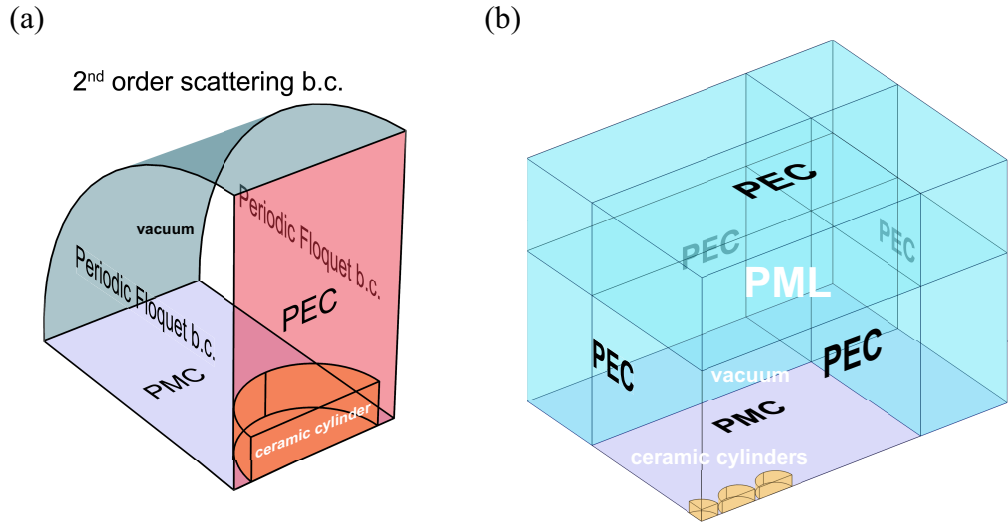


Figure 4 – (a) Schematic representation of the computational domain for calculating dispersion diagrams for a chain of ceramic cylinder. (b) Schematic representation of the computational domain for eigenfrequency simulations of a finite chain of ceramic cylinders.

In the case of finite chains, a high level of calculation accuracy is required, together with the lowest possible reflection from boundaries. In this case, the accuracy achieved with scattering boundary conditions is often insufficient, even when second-order boundary conditions are used. In such a case, the computational region is divided into two subregions, the background and the absorbing region connected to it, called perfectly matched layers PMLs). In this way the complex eigenfrequencies were found. The size of the background distance and the thickness of the PMLs can affect the resulting eigenfrequencies, especially the imaginary part, which was the main goal in our simulations. Therefore, we have performed the study of the dependence of the Q -factor on these parameters, and found the optimal values, which allow to achieve high enough accuracy of the obtained Q -factor, without making the computational domain too large. Moreover, in order to simplify the computational complexity and to reduce the number of calculated modes, we have made use of the symmetry planes. In this problem it is possible to distinguish all three symmetry planes, since we consider a chain of cylinders without a substrate. As it will be shown further, the mode of the interest corresponds to the magnetic-dipole Mie-resonances excited in the cylinders, with the dipole moment directed along the axis of the cylinder. According to the type of this mode we have chosen PMC type boundary conditions for the horizontal plane and PEC type symmetry plane for the vertical plane (along the chain axis).

An example of the computational domain for eigenfrequency simulations of a finite ceramic chain of 5 disks is shown in Fig 4(b).

Calculations of the optical chain were performed in a similar way. Most of the calculations of the coaxial chain of ceramic disks were performed in 2D axisymmetric geometry, which allowed us to fix the azimuthal number.

To calculate the scattering parameters and to optimize the experimental conditions the CST Studio Suite software was used. The calculations were performed in the frequency domain. Two shielded loop antenna models, closely reproducing the geometry of the real antennas used in the experiment, were used to simulate excitation and signal collection sources. The signal was input to one of the antennas using a waveguide port, while the other antenna was used for signal collection. To achieve a sufficient level of accuracy, PML was used as open boundary conditions. Also, the size of the mesh elements had a significant influence on the results obtained, thus a mesh with 10 elements per wavelength was used in the calculations. An illustration of the model used to simulate the scattering parameters of a ceramic chain of 5 cylinders is shown in Fig 5.

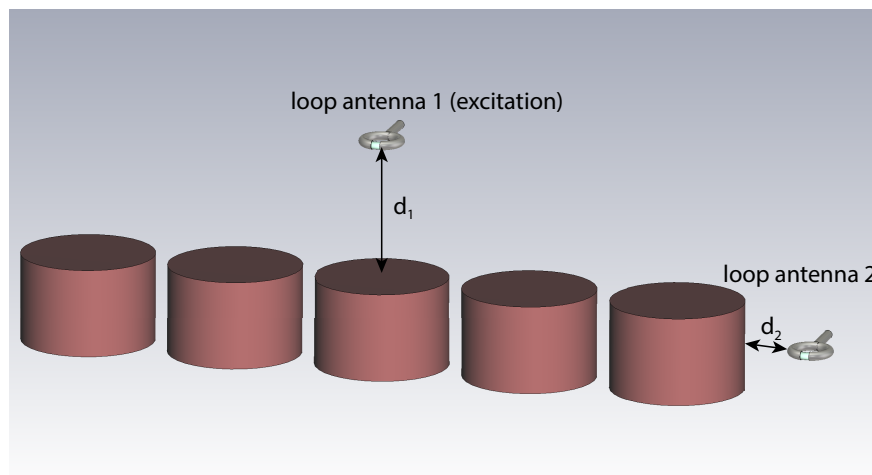


Figure 5 – Schematic representation of a chain of 5 cylinders and two loop antennas for signal excitation and collection, positioned at distances d_1 and d_2 respectively.

To analyze the obtained spectral dependencies (both calculated and experimental) and to extract useful data from them in order to determine the quality factor of the resonance, especially in the case of several closely interacting resonances, a program was written in the Python programming language. The program used the function “curve_fit”, which is part of the “scipy.optimize” package of the SciPy library. The “curve_fit” function uses a non-linear least squares method to fit a

user-defined function to a data. One or a sum of several Lorentzian-type functions typical for the observed resonance phenomena was used as a fitting function, discussed in more detail in the Section 2.2.

1.3.3 Experimental methods

To experimentally verify the effect, spectral measurements of the scattering parameters (S-parameters) were performed. For a resonant structure, the presence of resonant peaks corresponding to the modes of the structure is expected in the spectral dependencies of the S_{21} parameter. Excitation of modes in a chain can be done via near-field coupling of the source to the chain. To excite the magnetic-dipole mode of interest a shielded loop antenna that can be viewed as a magnetic-dipole source was used. The same antenna was used for the signal collection. For a chain consisting of even number of cylinders the antennas were placed at the edges of the chain at a distance of 1 cm from the cylinder, in order to reduce the coupling strength between the antenna and the cylinders, which reduces the influence on the measured parameters. For a chain consisting of an odd number of cylinders, one of the antennas was placed over the central disk, and the other antenna was placed on the side of the chain, which allowed us to excite the mode of interest. The antennas were connected to the corresponding ports on the Rohde & Schwarz vector network analyser (VNA). The experimental setup for measuring a chain of a 5 cylinders is shown schematically in Fig. 6.

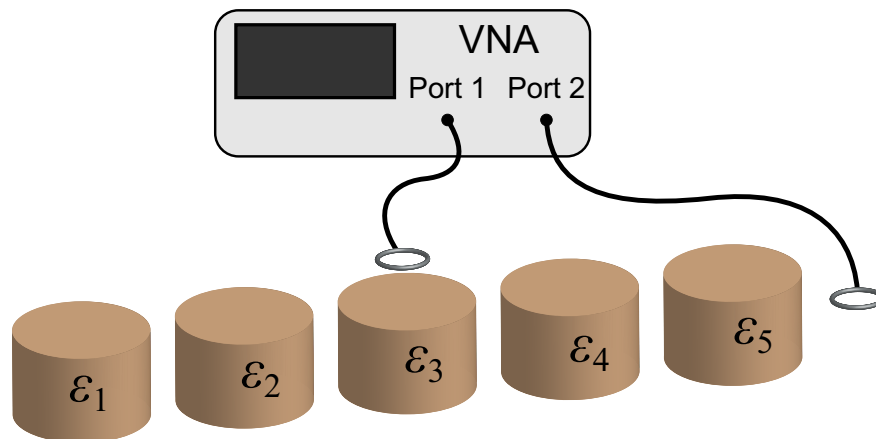


Figure 6 – Schematic of the experimental setup to measure the S_{21} parameter for a chain of 5 cylinders. In reality, the dielectric permittivities of individual cylinders may differ, even very slightly, which still influences the effect under study.

Conclusions on Chapter 1

In this chapter we have reviewed the main trends in the designs of dielectric optical resonators and highlighted their main advantages and drawbacks. We have argued that the resonances supported by the chain of dielectric resonators that emerge due to interaction of collective modes of the chain via radiation continuum are of interest in this context. We have described the main theoretical background on the formation and characteristics of such resonances. And we have described theoretical and experimental methods that allow for study of the structures supporting such modes.

2 CHAIN OF COUPLED CERAMIC RESONATORS

2.1 Analysis of the material and geometrical parameters required for experimental observation

During the analysis of how the geometrical and material parameters affect the possibility of achieving interference of the collective modes via radiation continuum and observation of this effect in experiment we have identified several important factors.

1) The permittivity of the material of the resonators mainly affects the degree of overlapping of different modes in the infinite chain of resonators. High permittivity allows to spectrally separate different modes of the individual resonators and correspondingly different bands of the infinite chain. This facilitates experimental observation of the chain characteristics. On the other hand, for small values of the permittivity, the different bands can mix with each other, which complicates the interference mechanism and its experimental observation and can even destroy the considered effect.

2) Material loss is one of the main parameters that affects the ratio of the radiative and nonradiative decay rates of the chain eigenmode. The minimal tangent loss of the ceramic materials with high enough permittivity is of the order of 10^{-5} - 10^{-4} . Depending on the value of the resulting quality factor, the nonradiative decay rate was dominating for the number of the resonators 6-10 in the chain. This was the main limiting factor in our experiments.

3) From the theoretical point of view the shape of the resonators did not matter substantially, and potentially the effect could be realized with the resonators of any shape. However, according to the theoretical predictions [21], the distance between the centers of the resonators should be small enough to ensure the appropriate coupling between them. This means that the size of the resonator in the direction of the chain axis should be several (at least approximately 4) times smaller than the resonant wavelength. This is easily achieved for one of the fundamental modes of the chain with high enough permittivity. For not very high permittivity and/or for the higher order modes of the chain one should rely on the anisotropic shape of the resonator such that the size in the direction of the chain axis is larger than transverse dimensions. Furthermore, since the ceramic resonators are often fabricated in the cylindrical shape, we have chosen to work with the resonators of such shape.

4) In order to avoid the complications caused by the mixing and spectral overlapping of the desired mode with other modes supported by the structure, we have focused on one of the fundamental modes of the chains of high index dielectric resonators. For the cylinders with not extreme aspect ratio these modes are magnetic and/or electric dipole modes, i.e. in which each of the resonators supports oscillations of the dipolar type. Furthermore, the effect is expected only for the modes with dipole moments oscillating in the direction transverse to the chain axis.

5) Following the previous point we were able to estimate the approximate dimensions of the cylindrical resonators that support dipole modes with transverse orientation and whose size in the direction of chain axis does not exceed approximately one fourth of the resonant wavelength. Such resonators were further the basic elements for the chain resonators.

As the result of numerical simulations that take into account all above mentioned factors, we have developed several potential designs based on the ceramic cylinders readily available in our lab. Mainly due to technical reasons we have performed experiments only with one of these designs described in the next section.

2.2 Results of numerical simulations

From what follows, in the main part of the simulations and the experiment we have focused on the chain of ceramic cylinders with the following parameters: height of the cylinders $h = 20$ mm, and radius of the cylinders $r = 15$ mm. The period of the chain was varied in the range $a \approx 30-45$ mm. As it will be shown further the resonant wavelength of the considered mode will be $\lambda_0 \approx 200$ mm, which makes the considered values of period approximately 5-6 times less. The relative permittivity of the ceramic material was chosen $\varepsilon = 44.8$. The material losses in ceramics were described by the dissipation factor (or loss tangent) $\tan \delta = \text{Im}(\varepsilon)/\text{Re}(\varepsilon)$, taking characteristic values in the range from 1×10^{-5} to 1×10^{-3} . A schematic representation of the cylinder chain is shown in Figure 7.

At the first step, we have analyzed the response of the individual cylinder. We have used COMSOL Multiphysics to find the eigenmodes of the cylinder. Further, knowing the symmetry of the mode we were able to excite these modes with a plane wave with proper direction of propagation and polarization and to perform multipole decomposition of the excited modes, according to the method de-

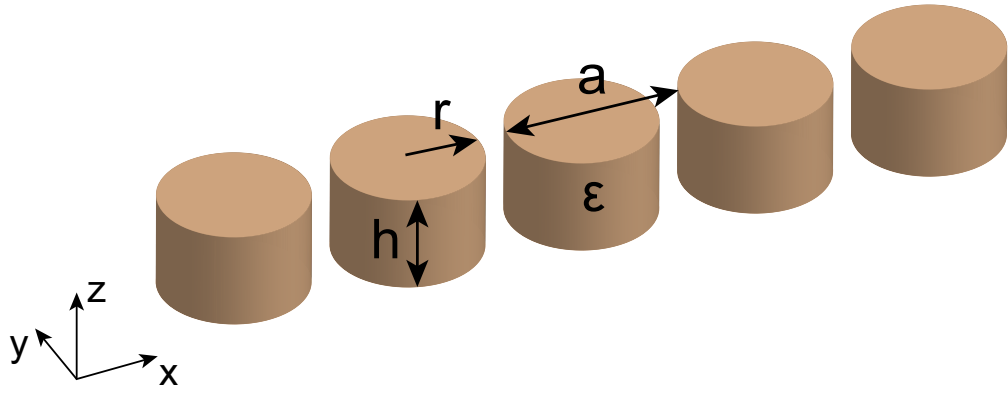


Figure 7 – Schematic of the chain of ceramic cylinders studies in this work.

scribed in the section 1.3.1. As an example, in Figure 8 we show the scattering cross-section and corresponding multipole decomposition for a plane wave incident along the diameter of the cylinder with a magnetic field polarized along the axis of the cylinder. For such excitation, in the scattering spectrum in the given spectral range we observed magnetic dipole modes with magnetic dipole moment oriented along the axis of the cylinder and electric dipole mode with electric dipole moment oriented along the diameter of the cylinder. In general, the simulations have shown that at least first few resonances are well separated in frequency and are characterized by a single dominant multipole contribution. Thus we expect the modes of the chain of the cylinders to be formed by coupled multipoles of a single type.

At the second step, we have performed numerical calculations of the dispersion curves of the infinite chain, in order to find the range of values of the chain period, in which they exhibit nonmonotonic behaviour. The simulations were also performed in COMSOL Multiphysics. The dispersion diagram for an infinite chain for a period $a = 32$ mm is shown in Figure 9(a). The black dashed line is the light line. We observe that the chain supports a lot of waveguide modes of different types. At least first three modes are well separated spectrally below the light line. This is achieved due to rather large quality factor of the resonances in a single cylinder and rather strong coupling between the cylinders in the chain. Such behaviour helps us to distinguish the modes of different type in the corresponding finite chains in experiment.

The variation of the period revealed that few of these modes can have non-monotonic character. We have focused of the fundamental mode that is formed due to coupling magnetic dipole resonances in individual cylinders. Dispersion

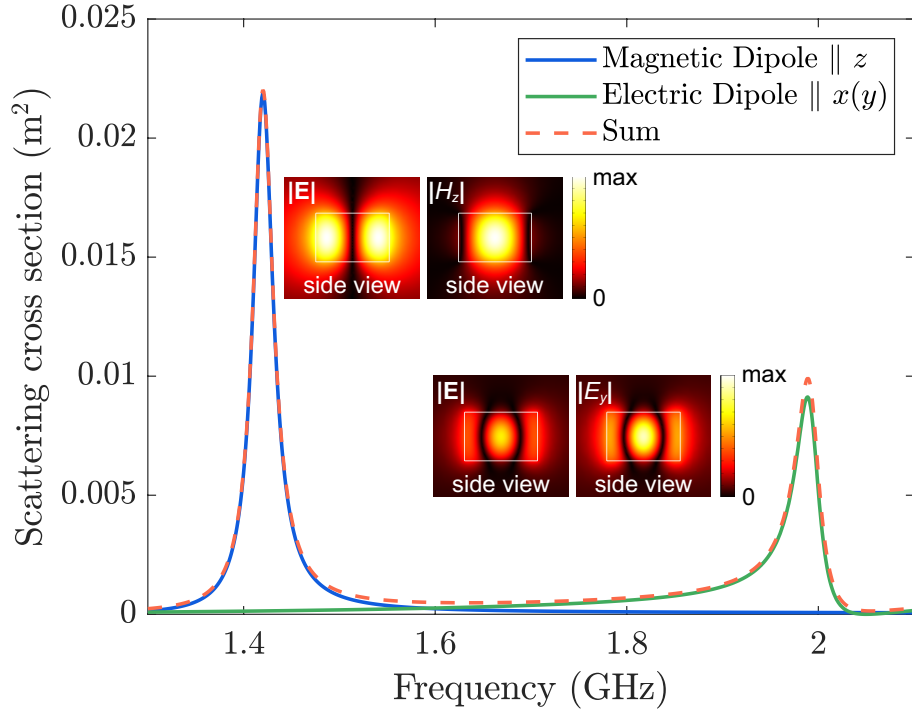


Figure 8 – Multipole decomposition of a single cylinder, the insets show the field distributions in the lateral cross section of the cylinder for the two Mie-resonances, magnetic dipole and electric dipole respectively.

diagrams for this mode, calculated for different values of period a , are shown in Figure 9(b). The inset of Figure 9(b) shows the distribution of the absolute value of the out-of-plane magnetic field component and the absolute value of the electric field in the lateral cross-section of the cylinder. As one can see from Figure 2(b), when the period of the chain is greater than a_{cr} , the dispersion curve of the first resonant mode is monotonic. Then, as the period of the chain decreases, the dispersion curve changes its behaviour, becoming nonmonotonic, starting from some value of period $a < a_{cr}$. Once the dispersion curve becomes nonmonotonic, moving on to the finite chain, a high- Q collective mode is expected to be formed.

After estimation of the parameters of the chain that allow for observation of the interacting collective modes, we have performed the calculations of the quality factor of the finite chain eigenmodes. For finite chains one expects to observe Fabry–Pérot resonances at the frequencies related to the wavenumbers through the dispersion of the infinite chain as follows:

$$\frac{qa}{\pi} = 1 - \frac{\xi}{N+1}, \quad (14)$$

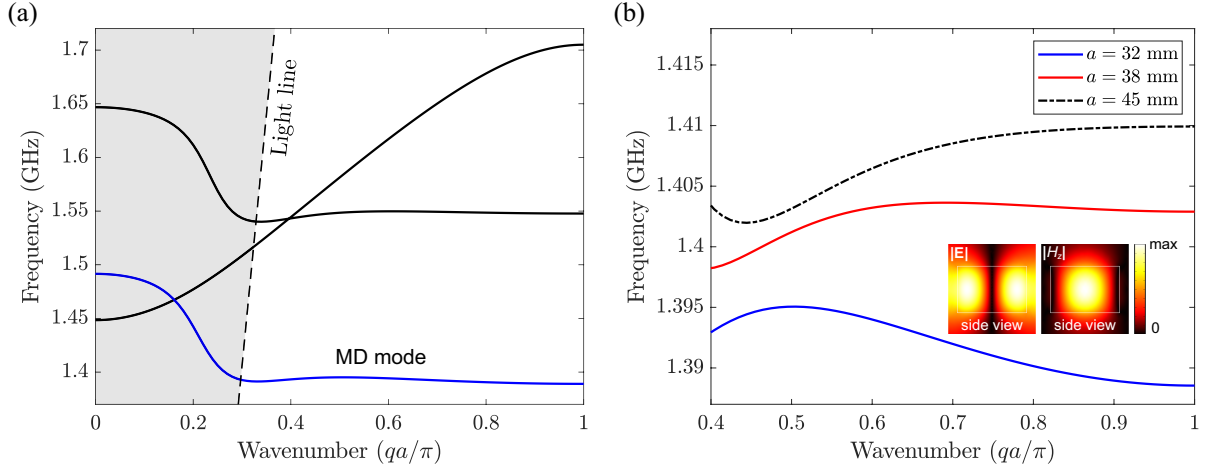


Figure 9 – (a) Dispersion diagrams for an infinite chain for period $a = 32$ mm, (b) Dispersion diagram of the first resonant mode of the chain for the different values of period.

where q is the Bloch wave number, a is the period, ξ is the number of resonance, N is the number of resonators in the system [31]. Therefore, for a period $a = 38$ mm, the inflection point of the dispersion curve corresponds to $qa/\pi \approx 0.7$, which allows us to expect the appearance of the high- Q mode in a finite chain of 5-6 resonators.

In order to find the parameters at which the formation of high- Q collective mode is observed, we have calculated the dependence of the total Q -factor on the the period of the chain a in the range 32-45 mm near the value of 38 mm expected from the analysis of the infinite chain. The results for a chain consisting of 5 cylinders are shown in Fig. 10(a).

We can notice that for a certain value of the period the radiative losses are seriously suppressed and, accordingly, the Q -factor reaches a certain maximum value, which according to the theory [5] indicates the interference of two collective modes of the chain. Calculations for $\tan \delta = 1 \times 10^{-4}$ show that even at this value of material losses the studied effect is still observed. Further, performing similar calculations for different number of cylinders in the chain, we obtain the dependence of the maximum quality factor for the corresponding number of cylinders in the chain, which is shown in Fig. 10(b). For calculations in case of absence of material losses, we can see that starting from 5-6 cylinders in the chain the quality factor grows as $Q \propto N^{\sim 7}$, which is in full correspondence with theoretical

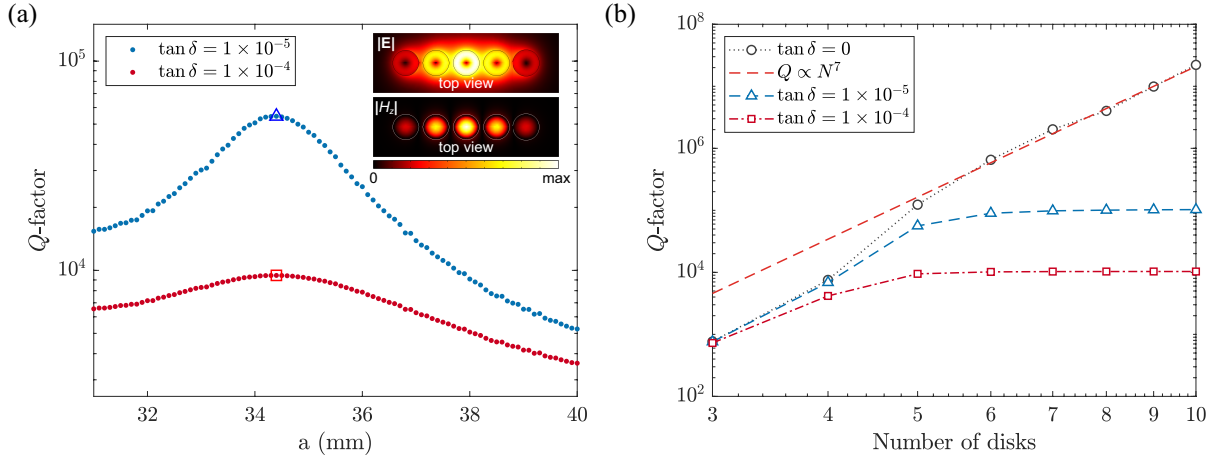


Figure 10 – (a) Dependence of the Q -factor on the distance a for a finite chain of 5 cylinders. The two curves correspond to different values of the material losses, the peak values of the Q -factor are marked on the curves by a triangle and a square respectively. The inset shows the distribution of the total electric field and the absolute value of the out-of-plane magnetic field component respectively in the horizontal cross section of the chain for the maximum Q -factor. (b) The obtained dependence of the maximum Q -factor on the number of resonators in the chain. Different curves correspond to different values of material losses. It can be seen that for a lossless chain starting from 5 disks the Q -factor grows as $Q \propto N^7$.

works [5, 21]. For the case of non-zero material losses a saturation is observed in the values of maximum possible Q -factor for the chain starting from 5-6 cylinders.

At this point the parameters of the chain were optimized and in order to proceed to the experimental verification of the effect we have done numerical calculation and optimization of the characteristics of the structure according to the experimental setup. For this purpose, we have calculated the scattering parameters (S-parameters) of the chain in the CST Studio Suite software. The simulation model is presented in Fig. 5.

Since the main multipole in the high- Q collective mode under study is a magnetic dipole with the dipole moment directed along the cylinder axis, we have chosen the loop antennas for excitation of the mode and collection the signal. For a chain consisting of odd number of cylinders, placing the source antenna above the central disk, only modes of a certain parity will be excited. Position of the antenna that collects the signal can be almost arbitrary as long as it has no significant influence on the mode. In the current setup we have placed it at the edge of the chain, as shown in Figure 5. Due to high Q -factor of the considered mode and well spectral separation of the other modes of the chain, we expect a single resonant peak in

the spectral dependence of the S_{21} parameter that corresponds to this mode. The spectrum of $|S_{21}|^2$ for a resonant structure in the single resonance approximation has the following form [32]:

$$|S_{21}|^2(\omega) = \left| \frac{ae^{i\varphi}}{\omega - \omega_0 + i(a + \gamma_{\text{NR}} + \gamma_{\text{rad}})} \right|^2, \quad (15)$$

where a is the coupling constant between the mode of the structure and the port, φ is the resonance phase, ω is the frequency of input signal, ω_0 is the resonant frequency of the structure, γ_{NR} and γ_{rad} is the nonradiative and radiative losses for the excited eigenmode, respectively. The coupling constant can be considered as an additional channel for radiative losses, whereas working with high-index ceramics we can expect γ_{NR} values to be approximately the same for all modes, as the fields are strongly confined within the disks. The distance at which we place the antennas from the chain is a parameter that must be optimized because it directly affects the coupling strength of the antenna and mode of the chain. Too close location of the antenna, and therefore, strong coupling between the antenna and the mode will significantly affect the values of the extracted Q -factor values, being an additional channel of losses. The coupling strength with the antenna for excitation positioned above the disk will be greater than the coupling strength with the signal collection antenna positioned at the edge, as the coupling is determined by the amount of overlap between the source field (in our case a loop antenna) and the mode of the resonant structure. Next, we are interested in working in weak coupling regime $a \ll \gamma_{\text{NR}} + \gamma_{\text{rad}}$, which would be characterized by the fact that the extracted values of the Q -factor would not depend on the position of the antenna.

By fixing the signal collection antenna at a distance $d_2 = 10$ mm from the edge of the chain, calculations of S_{21} parameter for different distances to the antenna for excitation d_1 for different values of the material losses were performed. Fig. 11(a) shows examples of the different spectra obtained. It can be seen that the half-width of the resonance curve decreases as the distance to the antenna increases, indicating an increase of the Q -factor. After processing the obtained spectra, the extracted Q -factor values were plotted from the distance to the excitation port as shown in Fig. 11(b). Starting from a certain distance d_1 , the extracted Q -factor values do not depend significantly on the antenna position, which indicates the transition to the weak coupling regime and, as a consequence, the minimization

of radiative losses. Moreover, it is worth noting that the extracted Q -factor values are in very good accordance with the values obtained in the eigenvalue simulations.

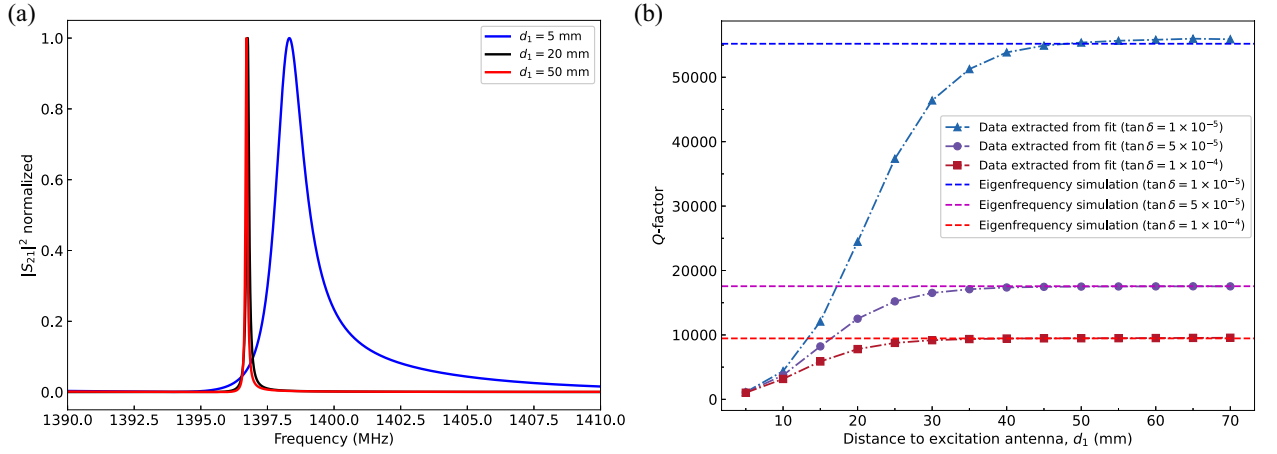


Figure 11 – (a) Examples of the calculated spectra of the S_{21} parameter for a chain of 5 cylinders, obtained for different values of the distance to the excitation antenna d_1 . (b) Obtained dependencies of the Q -factor versus the distance to the excitation antenna, extracted from the calculated spectra for a fixed value of the distance between the centers of individual cylinders a . The chosen value of distance a corresponds to the maximum Q -factor. Different curves correspond to different values of material losses in ceramics. The horizontal lines indicate the values of maximum Q -factor calculated in the eigenfrequency simulation.

Further, in order to verify that the chosen method is correct and we can obtain the Q -factor values very close to the calculated in eigenfrequency simulation, the S_{21} parameter was calculated for different distances between individual resonators in the chain and for different values of material losses. The excitation antenna distance was chosen $d_1 = 50$ mm, based on previously obtained data about the weak coupling regime. Thus, Fig. 12 shows curves with dependencies Q versus a , obtained from eigenfrequency simulations, as well as curves composed from data obtained from processing the calculated spectra of the S_{21} parameter in the frequency domain.

2.3 Experimental verification

In order to confirm the predicted results experimentally we have performed the measurements of the spectral response of the finite chain of ceramic cylinders with various size of the period of the chain and different number of the cylinders. To control the gap between the cylinders in the chain, we have made a sample holder from Penoplex foam material by using a computer numerical control machine drilling, that allowed for creation a set of wells with different distances be-

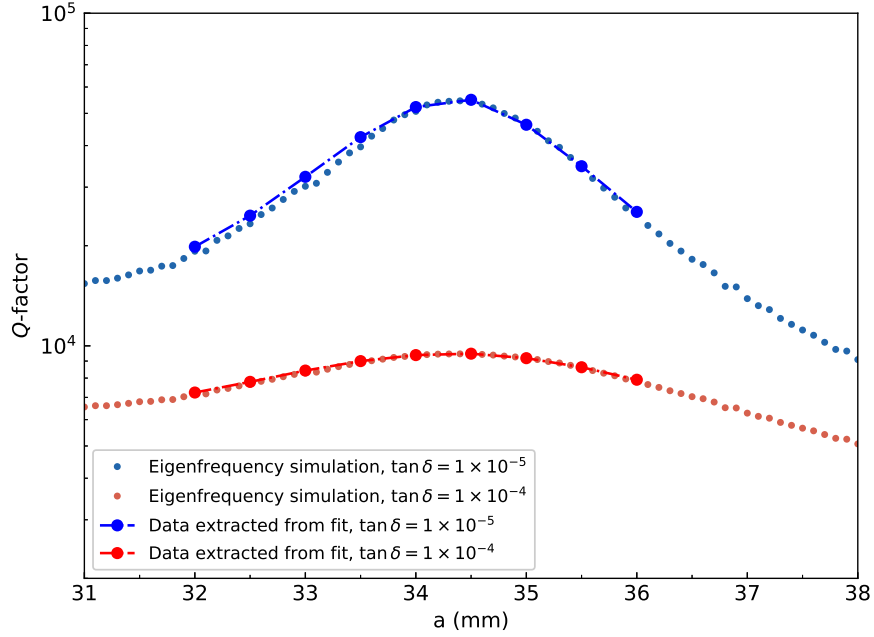


Figure 12 – Dependencies Q versus a for a chain of 5 cylinders, calculated for different values of material losses, together with the curves obtained from the data extracted from the calculated spectral dependencies of the S_{21} parameter.

tween the centers of wells, similar to distance a used in the simulations, ranging from 33 mm to 45 mm in 0.5 mm increments. The relative permittivity of Penoplex is practically 1 and material losses are negligible.

Various types of disorder, such as deviations in dielectric permittivity of individual cylinders in the chain, their position, defects, damage, etc. can have a significant influence on the formation of a high- Q band-edge mode. Deviations in cylinder positions are determined by the precision with which the corresponding positions in the sample holder are fabricated. Deviations in the dielectric permittivity values of individual cylinders will lead to changes in the resonant frequencies of the respective cylinders. In turn, this will affect both the maximum possible values of the Q -factor of the collective mode and the corresponding optimal values of the distance a . In order to determine the values of dielectric permittivity of individual cylinders in the chain, scattering parameters of each available cylinder were measured individually. For this purpose, two loop antennas were rigidly fixed on the sides of the cylinder at a distance of 5 mm. After the S_{21} parameter of all cylinders was measured, the resulting spectra were processed and the 5 cylinders with the closest resonance frequencies were selected. Moreover, the experimen-

tally determined resonant frequencies of the individual cylinder were compared with eigenfrequency simulations of a single cylinder with a variation of the relative dielectric permittivity of a ceramic in the range $\varepsilon = 43-45$ with steps of 0.01, which allowed for better estimation of the permittivity of the cylinders.

Next, we have performed the measurements of the S_{21} parameter for a chain of 5 cylinders. Examples of the experimental spectra are shown in Fig. 13(a). As expected, in the spectral dependencies one resonance peak with the characteristic Lorentzian-shape profile was observed. Further, we have extracted the Q -factors from all experimental spectra and have plotted the dependence of the measured Q versus a , as shown in Fig. 13(b). In order to compare the experimentally measured and numerically calculated characteristics of the chain we have done simulations of a chain of 5 cylinders taking into account the deviations in dielectric permittivity of individual cylinders, which were determined experimentally before. From such simulations we were able to determine a possible set of dielectric permittivities of each of the cylinders: $\varepsilon_i = \varepsilon + \delta\varepsilon_i$, where $\delta\varepsilon_1 = -0.08$, $\delta\varepsilon_2 = -0.11$, $\delta\varepsilon_3 = -0.16$, $\delta\varepsilon_4 = -0.08$, $\delta\varepsilon_5 = -0.07$; material losses were chosen to be the same for all cylinders as $\tan \delta = 5 \times 10^{-5}$. The resulting calculated curve for Q versus a is shown in Fig. 13(b). A quite good correspondence between the experimental and calculated data can be seen. Strongly differing experimental and calculated values at $a = 3$ mm, can be explained by feature of the holder construction for the antenna – the holder was fixed above the cylinder as a cap, tightly adjoining the neighboring cylinder at such small value of a . Thus, the contact with the holder walls could bring small deviations in positions of the central and neighboring cylinder, which led to significant influence on Q -factor of the mode. Differences of values near the peak can be related with the choice of not the most optimal measuring parameters, according to the previously obtained calculation data, i.e. it is due to the influence of insufficiently weak coupling between the antenna and the mode of the chain.

We have also performed the similar measurements for the chain consisted of 6 cylinders. In this case the vertical plane of symmetry perpendicular to the chain axis has magnetic type, and therefore, it is not possible to excite such a chain with a loop antenna with vertically oriented magnetic moment. We have decided to excite the chain from the side. In this case all modes irregardless of their parity can be excited. It turned out, that the second (with the second highest Q -factor)

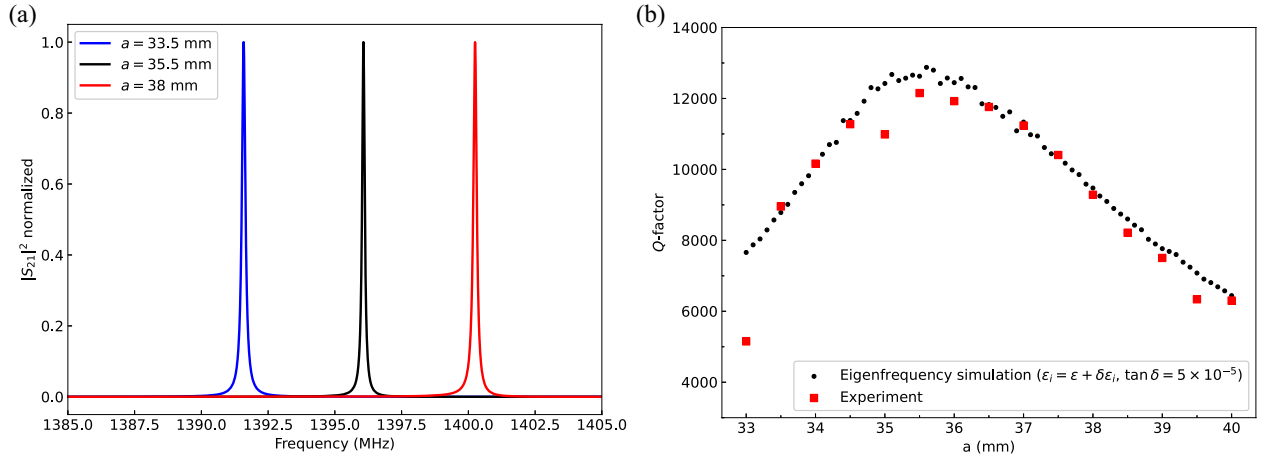


Figure 13 – (a) Examples of experimental spectra of the S_{21} parameter for a chain of 5 disks obtained for different values of distance a . (b) Experimental values of Q -factor versus the distance a together with results of numerical calculations taking into account deviations in values of dielectric permittivity of individual cylinders in a chain of 5 cylinders.

mode of the chain, which has different parity than the first mode (with the highest Q -factor), has the resonance frequency very close to the resonance frequency of the first mode. This is not a coincidence: according to the dispersion of the infinite chain we can predict the expected frequencies of all modes, assuming they do not interact. For large periods the dispersion is monotonic, and, therefore, the resonance frequency of the first mode is higher than that of the second mode. When the period decreases, for a certain value of the period the expected frequencies of the first and second mode become equal. However, due to interaction between the first and the third mode, their frequencies slightly shift. As a result, the frequencies of the first and the second mode intersect approximately for the value of the period, for which the first mode exhibits the highest Q -factor. In the experiment we excite all modes and the main contribution comes from the first and the second ones, since they have the highest Q -factors. Therefore, the resulting scattering spectrum represents a sum of two Lorentzian-type peaks (or more than two if one wants to take into account weak contribution from other modes). In order to extract the values of the Q -factors of all excited modes, we have fitted the measured spectra with the following function:

$$|S_{21}|^2(\omega) = \left| \sum_j \frac{a_j e^{i\varphi_j}}{\omega - \omega_{0j} + i(a_j + \gamma_{NR_j} + \gamma_{rad_j})} \right|^2, \quad (16)$$

where index j determines the excited mode, and the total number of excited modes depends on the specific parameters; in our simulations it was typically enough to take into account 2 or maximum 3 modes. The obtained results are shown in Figure 14(a). However, it was not known beforehand which of the extracted Q -factors belongs to which type of the mode. In order to make this distinction we have also plotted the resonance frequencies of these modes in Figure 14(b). It turned out that these modes exhibit anticrossing behaviour, although they are supposed to have different parity, which is confirmed by the correspondence between their large values of the measured and calculated Q -factors. From this plot, we were able to divide these two modes, and to observe the expected maximum of the Q -factor for one of the mode for approximately the same period as in the simulations. The maximal Q -factor was approximately the same as for the chain of 5 cylinders, indicating that the non-radiative part of the losses indeed become dominant even for such small values of the number of the resonators in the chain. The exact origin of the interaction of the first and second mode remained unclear, although it should be related with the breaking of the symmetry either by the exciting and receiving antennas, or by the defect in the resonators or the holder.

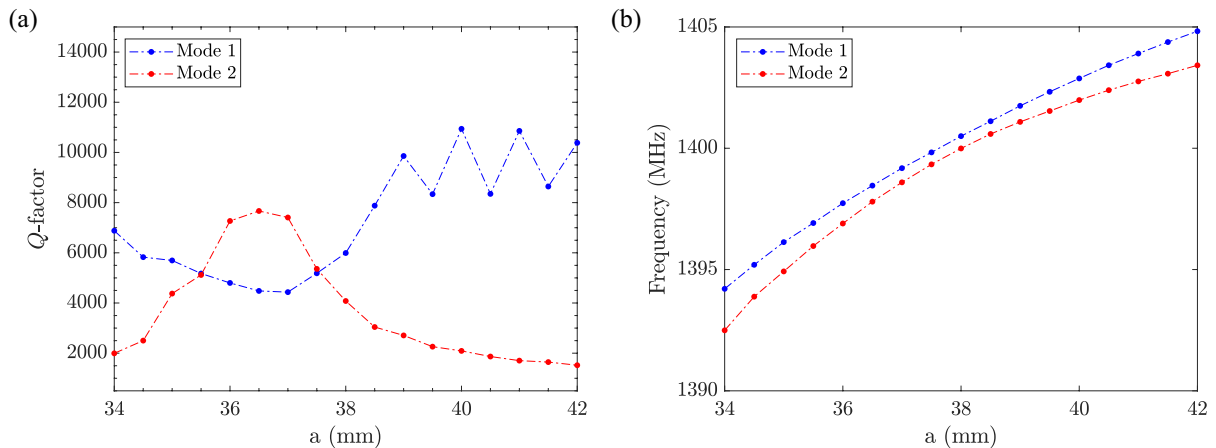


Figure 14 – (a) Quality factors and (b) resonance frequencies of two modes extracted from the measured S_{21} parameters for the chain of 6 ceramic cylinders.

2.4 Chain of ceramic cylinders in coaxial arrangement

One of the major problems in experimental observation of the interaction of the modes was rather strong material losses of the employed ceramic material. Because of the characteristic field distribution in the case of magnetic dipole resonances mostly localized inside the resonators the Q -factor of the collective modes saturates even for 5-6 resonators in the chain. Since the available ceramic materials

always exhibit tangent loss on the level 10^{-5} - 10^{-4} minimum, we have decided to consider higher order type of modes, which might have higher fraction of electric energy stored in the gaps rather than inside dielectric. We were able to identify such kind of modes in a chain composed of the same ceramic disks as the one considered earlier but with the disks arranged coaxially, as schematically shown in Fig.15. Having axial symmetry, this problem was considered in 2D axisymmetric geometry, with the possibility to fix the azimuthal number m in the simulations. For this arrangement of resonators a number of features can be noted:

- The limitation on the distance between individual resonators in a chain in this case is the height of the cylinder, which can potentially increase the coupling strength of individual resonators in a chain by bringing the resonators closer together than in the previously considered case.

- Considering the resonant modes in which the Mie-resonance of dipole type dominates, one can expect the appearance of a strong coupling between the modes, with the dipole moment oriented along the radius of the cylinder. This can be explained by the fact that the coupling between individual resonators in the chain is achieved through the near-field interaction, hence for dipoles oriented along the cylinder radius ($m = 1$), one can just expect strong overlap of fields and effective emission along the chain axis.

- From the previous point as it is possible to expect occurrence of “hotspots” and strong confinement of a field in gaps between cylinders, that in turn can reduce influence of material losses of ceramics on maximum Q -factors of collective modes.

Thus, following similar procedure as described earlier, we began our analysis of the structure by considering an infinite chain since the mode structure and multipole analysis for the single resonator were performed earlier. The dispersion diagram calculated in 3D geometry without fixing the azimuthal number is shown in Fig. 16. At the initial stage, this allowed us to get a complete picture of the mode structure of the chain. As expected, for modes with azimuthal number $m = 1$, we found the first resonant mode, with nonmonotonic dispersion, which is shown in Fig. 16 by yellow curve. Also note that the modes are twice degenerate and we observe two close curves. The dominant contribution in this mode is the electric dipole Mi-resonance, and it can also be seen on the scattering spectrum with the multipole analysis performed near the 2 GHz region, presented earlier in Fig.8.

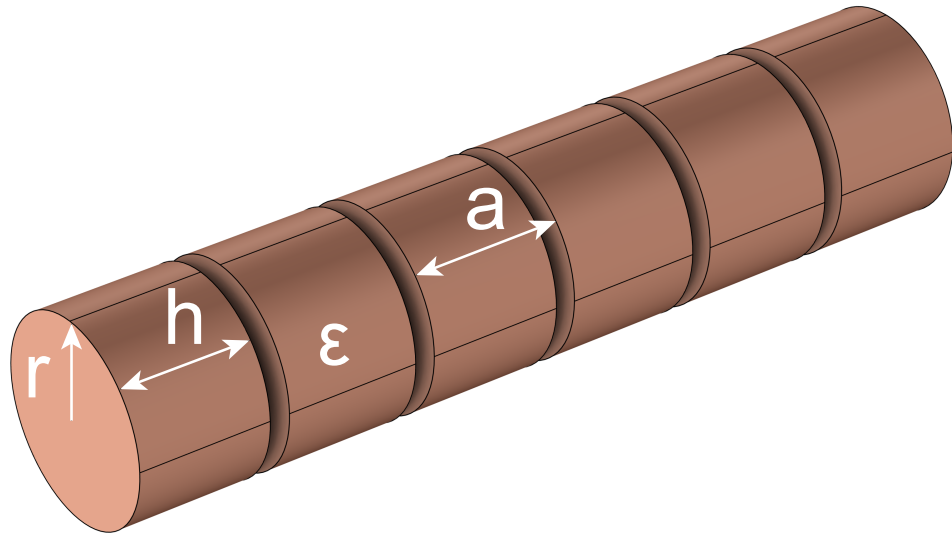


Figure 15 – Schematic representation of a chain of ceramic cylinders with parameters $r = 15$ mm, $h = 20$ mm in coaxial arrangement

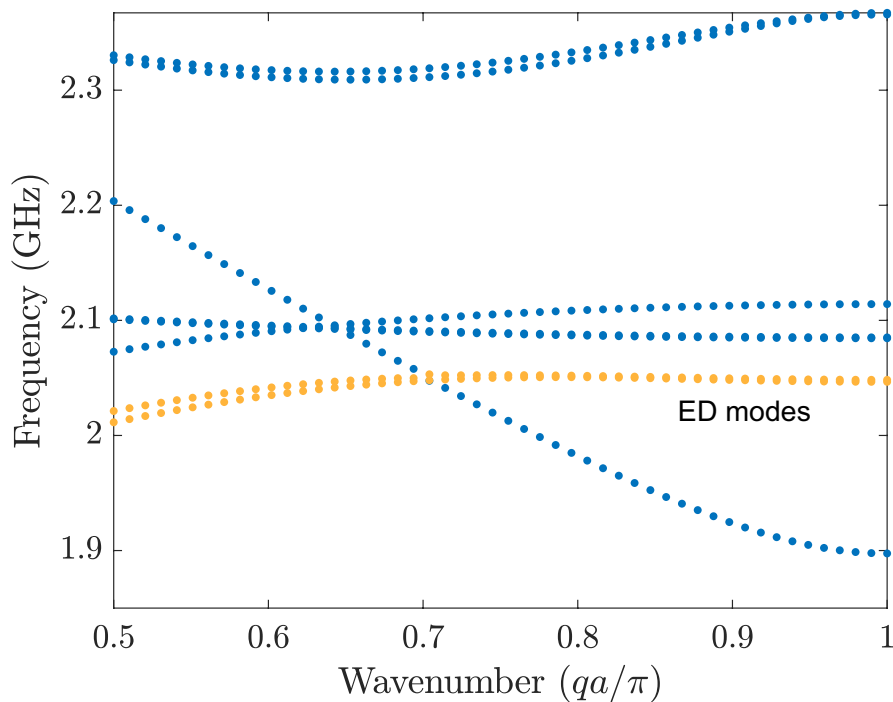


Figure 16 – Dispersion diagram of the coaxial chain calculated for $a = 22.6$ mm.

Next, by moving to 2D axisymmetric geometry and fixing the azimuthal number $m = 1$, the dispersion curves for the mode found earlier were calculated for various periods of the chain, as shown in Fig. 17(a). Another significant difference

can be noted here: the range of values of the period in which the non-monotonic behaviour of the dispersion curve is observed is much smaller compared to the previously considered configuration of the chain, and limited to only a few millimetres. From this we can also conclude that the maximum Q -factor of high- Q band-edge mode in this chain will be observed at very small distances between individual cylinders in the chain, hence the range of possible deviations in these distances becomes extremely small. This in turn will dramatically complicate the experimental verification of the effect. Fig 17(b) shows the field distribution in the side cross section of the chain.

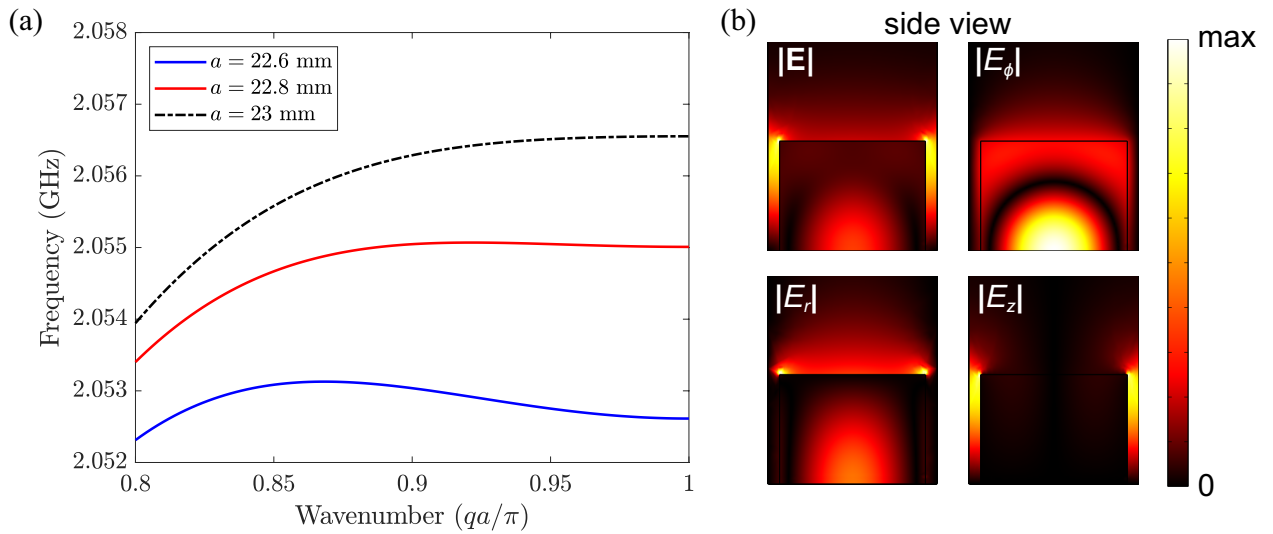


Figure 17 – (a) Dispersion curves corresponding to the eclectic dipole mode with azimuthal number $m = 1$ calculated for different values of period a . (b) Field distributions in the side cross section of the chain.

Next, finite chains were considered in order to determine the parameters at which the maximum Q -factor values are observed. Calculations Q versus a were performed, Fig. 18(a) shows the calculation for a chain of 6 cylinders for different values of material losses. We can see the presence of a maximum in the quality factor, and, as expected, the corresponding value of the optimum distance between the resonators is very small. The inset shows the distribution of the total electric field in the side cross section of the chain. Also note that when the distance a is changed by only a few tenths of a millimeter, the Q -factor values drops by approximately two orders of magnitude. At this point, we can already conclude that experimental verification of the effect in this configuration is extremely difficult, since positioning the individual resonators in the chain to within a hundredth of a millimeter is almost impossible. Moreover, random deviations in the positions, as

well as in the material parameters of the individual cylinders will cause an even more significant effect than in the previously considered configuration. Next, the dependence of the maximum Q -factor values on the number of cylinders in the chain was obtained, the results are shown in Fig. 18(b).

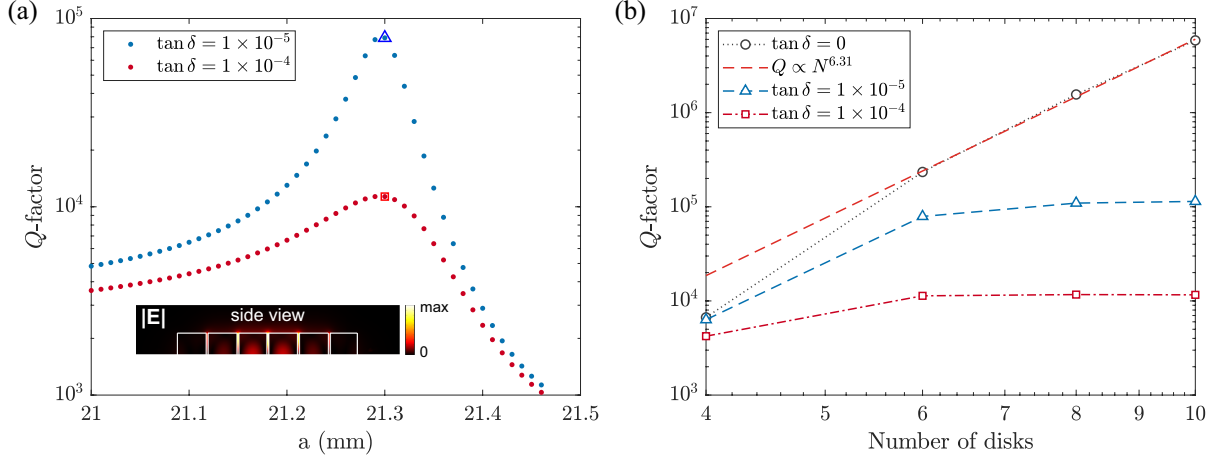


Figure 18 – (a) Dependence of the Q -factor on the distance a for a finite chain of 6 cylinders in coaxial arrangement. The two curves correspond to different values of the material losses, the peak values of the Q -factor are marked on the curves by a triangle and a square respectively. The inset shows the distribution of the total electric field in the side cross section of the chain for the maximum Q -factor. (b) The obtained dependence of the maximum Q -factor on the number of resonators in the chain. Different curves correspond to different values of material losses. Also the asymptotic dependence for the lossless chain is shown by the dashed line.

Note that the saturation in the Q -factor values starts from about 8 cylinders in the case of material losses $\tan \delta = 1 \times 10^{-5}$, which differs from the previous considered configuration (there the saturation was observed at 6 cylinders). However, the absolute values of the Q -factors are also different and reach slightly lower values compared to the previous configuration. There is also a significant difference in the asymptotic growth of Q -factor for the absence of material losses: starting from 6 resonators in the chain, the Q -factor grows as $Q \propto N^{\sim 6.3}$. For the earlier considered configuration the growth of $Q \propto N^{\sim 7}$ was observed, which was in full agreement with the theoretical data obtained for the dipole model [5]. Such modification of the power dependence might be related to the mixing of this mode with one of the higher-order modes and requires further investigation.

Conclusions on Chapter 2

In this chapter, two designs of a chain of ceramic cylinders were considered in order to optimize these structures for experimental verification of the formation of high quality band-edge modes. For both designs numerical calculations were performed in order to find high quality band-edge modes and to optimize the structure parameters. For the first considered design also experimental verification of the effect was performed, and the obtained experimental results are in good correspondence with the calculation results, with taking into account the influence of deviations in the material parameters of the real ceramics.

3 CHAIN OF COUPLED SILICON RESONATORS

In this chapter we discuss the design of a realistic dielectric optical structure that can be fabricated from silicon-on-insulator (SOI) wafers. Based on the design proposed in [5], the structure is a one-dimensional chain of silicon resonators in the shape of a rectangular prism placed on a silicon dioxide substrate. Numerical calculations of the optical resonant structure were performed similar to the calculations presented in Chapter 2. First the mode structure of the single resonator were analyzed, then the multipole analysis were performed. After that, calculations of the infinite and finite resonant structure were performed in order to find the parameters at which high- Q band-edge modes are observed. The two high- Q band-edge modes with the main magnetic dipole and magnetic quadrupole Mie-resonances were considered. The influence of the substrate was also analyzed.

A reasonable continuation of the study discussed in Chapter 2 is to develop a feasible design for an optical resonant structure that supports high quality band-edge modes. There is flexibility in the choice of geometric shape of the single resonators that will form the chain: cylindrical resonators as well as rectangular prism shaped resonators can be considered. Designs with both cylindrical [3, 4] and rectangular [2, 33] resonators have been experimentally realized, however, in all works the structures show formation of regular band-edge modes with characteristic growth of quality factor as $Q \propto N^3$. For the design proposed in [5] formation of high- Q band-edge modes has been demonstrated by optimizing the width of a single rectangular resonator. The use of resonators in the form of rectangular prisms can be justified, first, because such shape of the particles can be fabricated with conventional lithographic methods, second, because in this case there are several degrees of freedom, which allow for precise tuning of the structure parameters, and third, because the distance between the centers of the individual particles in the chain can be made rather small, which leads to both reduction of the length of the entire structure and the possibility of increasing the coupling strength between the resonators, which is required for the dispersion flattening. Also use of resonators in the shape of rectangular prisms allows to get rid of degeneracy of modes, which might be convenient for the experimental observations. Therefore, for further analysis a similar chain design was chosen, with the following geometrical parameters of individual resonator: $w = 200$ nm, $h = 600$ nm, $d = 550$ nm, schematically shown in Fig. 19. The choice of the height of the structure is due to

the availability of silicon wafer fabrication technology of the given thickness. The other two parameters are chosen for the reasons of the first resonant modes near $1.3 \mu\text{m}$, together with the reasons described earlier. An important difference in the approach used further from that used in [5] is to fix all geometrical parameters of an individual resonator and to vary the distance between individual resonators in the chain. In this way the mode structure and optical properties of an individual resonator remain unchanged.

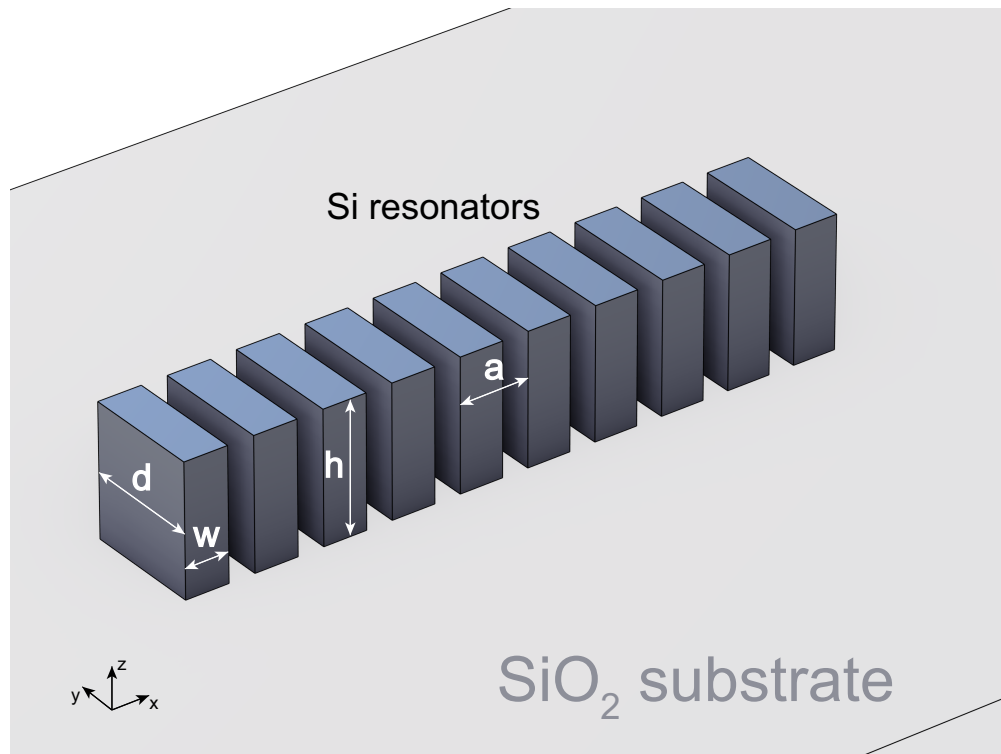


Figure 19 – Schematic representation of the optical resonant structure: a chain of silicon resonators on a silicon dioxide substrate

3.1 Results of numerical simulations

In the first step, the structure without a substrate was considered. Following the same reasoning as in Chapter 2, the analysis of the structure began by considering a single silicon resonator with the geometrical parameters $w = 200 \text{ nm}$, $h = 600 \text{ nm}$, $d = 550 \text{ nm}$ and the refractive index $n = 3.5$. The first resonant modes were found, and a multipole analysis of the scattering cross section spectrum was performed, the results of which are presented in Figure 20. The scattering of a x -polarized plane wave incident along the y -axis was considered. In the scattering spectrum one can see the presence of closely spaced resonant modes, with the main magnetic dipole and magnetic quadrupole Mie-resonances. The insets show

the distribution of the total electric field in the lateral cross section of the resonator for the magnetic dipole (left) and magnetic quadrupole (right) modes respectively.

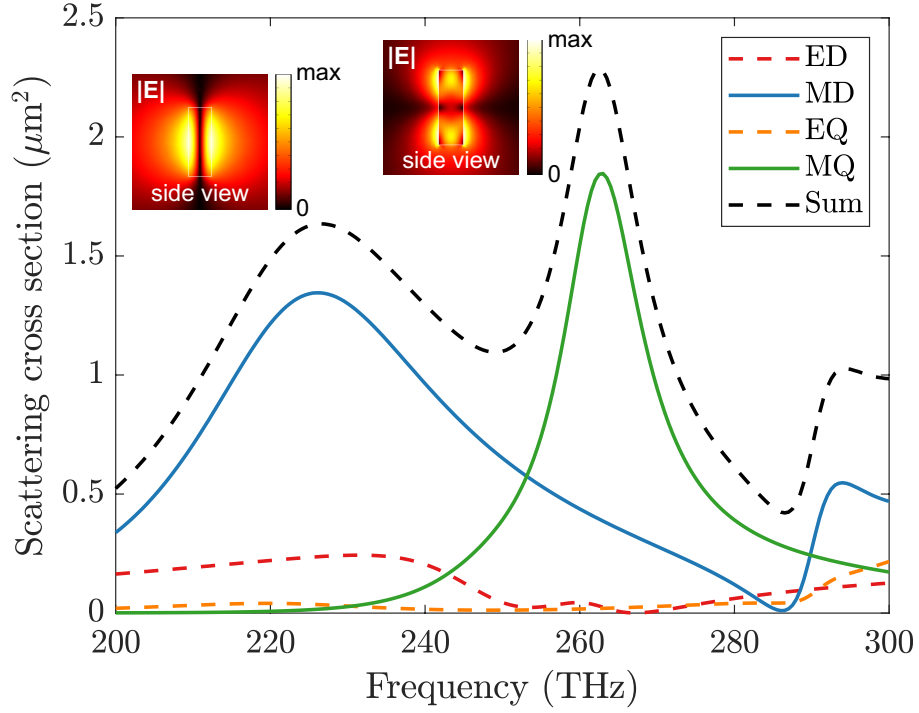


Figure 20 – Multipole decomposition of a single Si resonator in a vacuum, the insets show the field distributions in the lateral cross section of the resonator with dominant magnetic dipole and magnetic quadrupole Mie-resonances respectively.

Next, an infinite chain of resonators was considered. An example of a dispersion diagram calculated using the xz -electric (PEC) and xy -magnetic (PMC) symmetry planes is shown in Fig. 21(a). The second dispersion curve corresponds to the magnetic dipole mode, and for some values of period exhibit a nonmonotonic behaviour, as shown in Fig. 21(b). With further increase in period, the dispersion curve of this mode becomes monotonic. Hence, for period values at which the dispersion curve is nonmonotonic, we can expect the formation of high- Q band-edge modes in the case of finite chain.

Then a dispersion diagram using zx - and xy - PMC symmetry planes was calculated to analyze the magnetic quadrupole mode, the results are shown in Fig. 21(c). It is also seen that for similar values of period (Fig. 21(d)), the dispersion curve corresponding to the magnetic quadrupole mode is nonmonotonic, which also allows one to expect the formation of high quality collective modes in the finite chain.

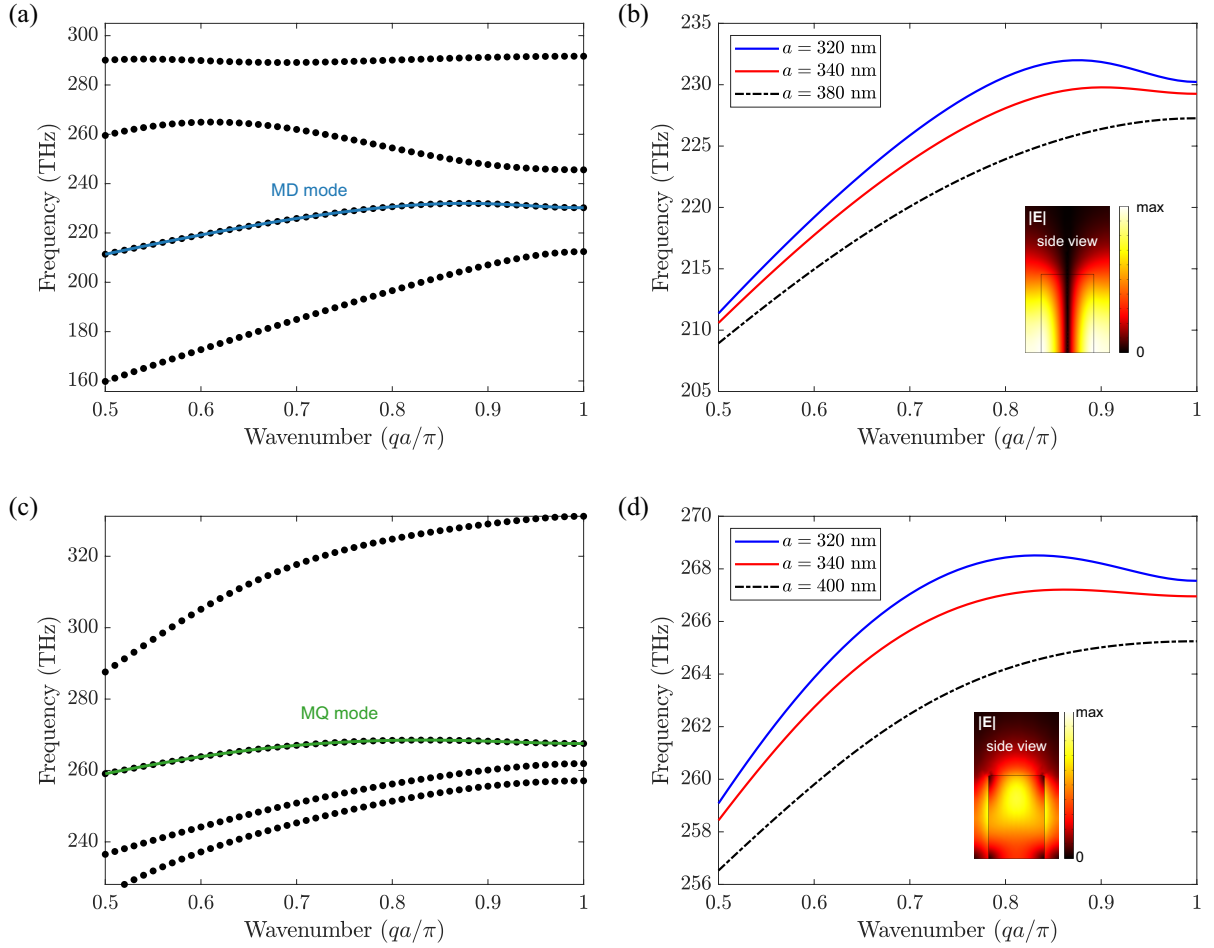


Figure 21 – (a) Dispersion diagram calculated using xz -electric and xy -magnetic symmetry planes for period $a = 320$ nm, the highlighted curve corresponds to the magnetic dipole mode. (b) Dispersion curves corresponding to the magnetic dipole mode calculated for different values of period a . (c) Dispersion diagram, calculated with xz - and xy - magnetic symmetry planes for period $a = 320$ nm, the marked curve corresponds to the magnetic quadrupole mode. (d) Dispersion curves corresponding to the magnetic quadrupole mode calculated for different values of period a .

Afterwards a finite chain was considered in order to find an optimal value of distance between resonators at which the highest quality factor of a collective mode is observed. So the numerical calculations of total Q -factor vs. the distance a , for both magnetic dipole and magnetic quadrupole modes were performed, an example of obtained dependence for a chain of 10 resonators without and with the substrate are presented in Figs. 22(a) and Figs. 23(a), respectively.

Conclusions on Chapter 3

In this chapter the design of a realistic optical resonance structure supporting high- Q band-edge modes was discussed. The proposed structure can support a set

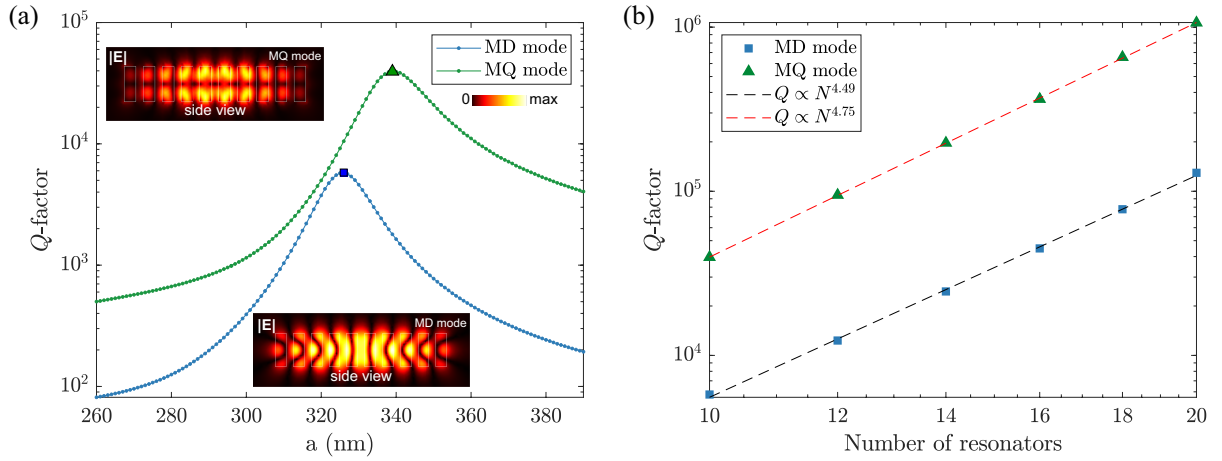


Figure 22 – (a) Dependencies Q -factor versus distance a , for two high- Q collective magnetic dipole and magnetic quadrupole modes respectively for the structure without substrate. The insets show distribution of total electric field in lateral cross section of the structure, for magnetic dipole and magnetic quadrupole modes, respectively, for the maximum Q -factor (also marked by a square and a triangle on the curves). (b) Dependence of maximum Q -factor values on the number of resonators in the chain for the two modes.

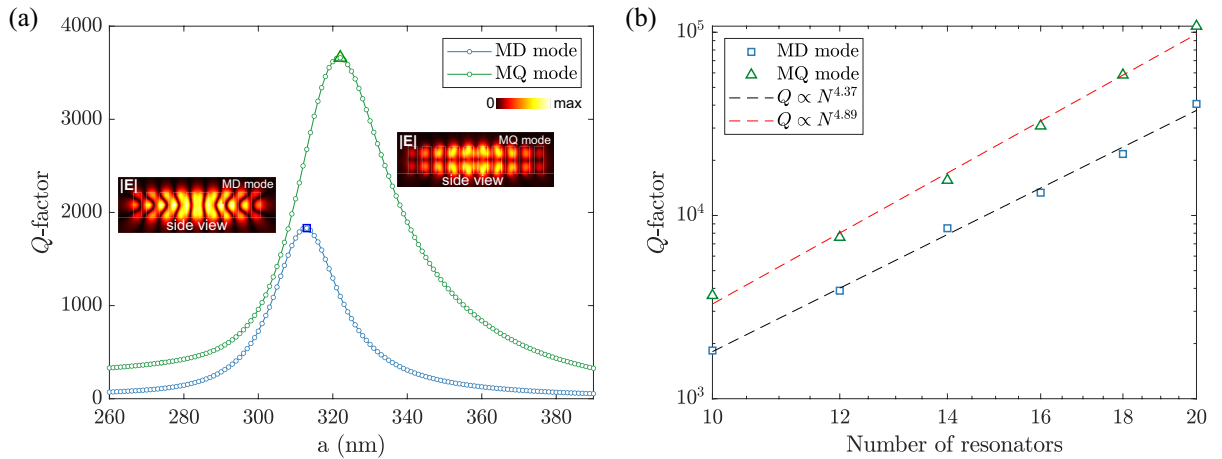


Figure 23 – (a) Dependencies Q -factor versus distance a , for two high- Q collective magnetic dipole and magnetic quadrupole modes respectively for the structure on a substrate. The insets show distribution of total electric field in lateral cross section of the structure, for magnetic dipole and magnetic quadrupole modes, respectively, for the maximum Q -factor (also marked by a square and a triangle on the curves). (b) Dependence of maximum Q -factor values on the number of resonators in the chain for the two modes.

of several high- Q collective modes at different frequencies with different dominant Mie-resonances, but with the same fixed parameters of the individual resonator in the chain. Thus, optimum values of distance between resonators, at which Q -factor of modes becomes maximal, also are different for each of modes. Maximum

quality factor obtained for magnetic quadrupole mode exceeds maximum quality factor for magnetic dipole mode in case of structure on substrate almost by two times. Also, compared to the magnetic dipole mode, a larger range of distances between individual resonators is observed for the magnetic quadrupole mode, at which the Q -factor starts to increase significantly. Also note that mode leakage into the substrate, being one of the main loss mechanisms in the case of an optical structure, does not critically affect the formation of a high- Q band-edge mode.

CONCLUSION

In summary, we have studied the chain of resonators that support band edge states with high quality factors enhanced due to coupling of two collective states via the radiation continuum. We have analyzed what kind of geometrical and material parameters allow to achieve such regime and developed a design of a chain of ceramic resonator operating in microwave spectral range that allows for experimental observation of this effect. The measurements performed for the developed design revealed that the Q -factor of one of the chain modes exhibits a maximum as a function of the period, which according to theory and simulations is the indication of the observation of the mode interaction. We have shown that even slightest deviations of the material and geometrical parameters of the chain as well as material losses may substantially reduce the Q -factor, which was the main limitation in the performed experiments. We have also shown theoretically that the predicted effect is quite general and can be observed for the mode of the resonator chain of any type. Our simulations revealed that the chain of silicon nanoresonators operating in optical frequency range possesses a mode with dominant magnetic quadrupole moments excited in the nanoresonators, which exhibits a maximum as a function of the period of the chain. Moreover, the Q -factor of this mode exceeds that of the dipole-type mode by approximately 1 order and allows for larger deviation of the value of the period from the optimal one, which can be advantageous for the future experiments.

REFERENCES

- 1 Guiding optical modes in chains of dielectric particles / G. S. Blaustein [et al.] // *Opt. Express*. — 2007. — Dec. — Vol. 15, no. 25. — P. 17380–17391. — ISSN 1094-4087. — DOI: 10.1364/OE.15.017380.
- 2 All-Optical Modulation in Chains of Silicon Nanoantennas / L. Ding [et al.] // *ACS Photonics*. — 2020. — Apr. — Vol. 7, no. 4. — P. 1001–1008. — DOI: 10.1021/acsp Photonics.9b01678.
- 3 Coupling of Germanium Quantum Dots with Collective Sub-radiant Modes of Silicon Nanopillar Arrays / V. Rutckaia [et al.] // *ACS Photonics*. — 2021. — Jan. — Vol. 8, no. 1. — P. 209–217. — DOI: 10.1021/acsp Photonics.0c01319.
- 4 Collective Mie Resonances for Directional On-Chip Nanolasers / T. X. Hoang [et al.] // *Nano Lett.* — 2020. — Aug. — Vol. 20, no. 8. — P. 5655–5661. — ISSN 1530-6984. — DOI: 10.1021/acs.nanolett.0c00403.
- 5 High- Q Localized States in Finite Arrays of Subwavelength Resonators / D. F. Kornovan [et al.] // *ACS Photonics*. — 2021. — Dec. — Vol. 8, no. 12. — P. 3627–3632. — DOI: 10.1021/acsp Photonics.1c01262.
- 6 Single-chip microprocessor that communicates directly using light / C. Sun [et al.] // *Nature*. — 2015. — Dec. — Vol. 528, no. 7583. — P. 534–538. — ISSN 1476-4687. — DOI: 10.1038/nature16454.
- 7 Ultrahigh- Q toroidal microresonators for cavity quantum electrodynamics / S. M. Spillane [et al.] // *Phys. Rev. A*. — 2005. — Jan. — Vol. 71, no. 1. — P. 013817. — ISSN 2469-9934. — DOI: 10.1103/PhysRevA.71.013817.
- 8 *Kippenberg T. J., Spillane S. M., Vahala K. J.* Demonstration of ultra-high- Q small mode volume toroid microcavities on a chip // *Appl. Phys. Lett.* — 2004. — Dec. — Vol. 85, no. 25. — P. 6113–6115. — ISSN 0003-6951. — DOI: 10.1063/1.1833556.
- 9 Integrated Whispering-Gallery-Mode Resonator for Solid-State Coherent Quantum Photonics / A. Brooks [et al.] // *Nano Lett.* — 2021. — Oct. — Vol. 21, no. 20. — P. 8707–8714. — ISSN 1530-6984. — DOI: 10.1021/acs.nanolett.1c02818.

- 10 Genetically designed L3 photonic crystal nanocavities with measured quality factor exceeding one million / Y. Lai [et al.] // *Appl. Phys. Lett.* — 2014. — June. — Vol. 104, no. 24. — P. 241101. — ISSN 0003-6951. — DOI: 10.1063/1.4882860.
- 11 Strong coupling between a photonic crystal nanobeam cavity and a single quantum dot / R. Ohta [et al.] // *Appl. Phys. Lett.* — 2011. — Apr. — Vol. 98, no. 17. — P. 173104. — ISSN 0003-6951. — DOI: 10.1063/1.3579535.
- 12 Bloch-Wave Engineering of Quantum Dot Micropillars for Cavity Quantum Electrodynamics Experiments / M. Lerner [et al.] // *Phys. Rev. Lett.* — 2012. — Jan. — Vol. 108, no. 5. — P. 057402. — ISSN 1079-7114. — DOI: 10.1103/PhysRevLett.108.057402.
- 13 Polarization-Resolved Plasmon-Modulated Emissions of Quantum Dots Coupled to Aluminum Dimers with Sub-20 nm Gaps / L. Tobing [et al.] // *ACS Photonics.* — 2018. — Apr. — Vol. 5, no. 4. — P. 1566–1574. — DOI: 10.1021/acsp Photonics.8b00009.
- 14 Plasmonic crystal defect nanolaser / A. M. Lakhani [et al.] // *Opt. Express.* — 2011. — Sept. — Vol. 19, no. 19. — P. 18237–18245. — ISSN 1094-4087. — DOI: 10.1364/OE.19.018237.
- 15 The photonic band edge laser: A new approach to gain enhancement / J. P. Dowling [et al.] // *J. Appl. Phys.* — 1994. — Feb. — Vol. 75, no. 4. — P. 1896–1899. — ISSN 0021-8979. — DOI: 10.1063/1.356336.
- 16 Low-threshold lasing at the edge of a photonic stop band in cholesteric liquid crystals / V. I. Kopp [et al.] // *Opt. Lett.* — 1998. — Nov. — Vol. 23, no. 21. — P. 1707–1709. — ISSN 1539-4794. — DOI: 10.1364/OL.23.001707.
- 17 Demonstration of the enhanced Purcell factor in all-dielectric structures / A. Krasnok [et al.] // *Appl. Phys. Lett.* — 2016. — May. — Vol. 108, no. 21. — P. 211105. — ISSN 0003-6951. — DOI: 10.1063/1.4952740.
- 18 Low loss waveguiding and slow light modes in coupled subwavelength silicon Mie resonators / L. Ding [et al.] // *Nanoscale.* — 2020. — Nov. — Vol. 12, no. 42. — P. 21713–21718. — ISSN 2040-3364. — DOI: 10.1039/D0NR05248E.

- 19 *Friedrich H., Wintgen D.* Interfering resonances and bound states in the continuum // *Phys. Rev. A.* — 1985. — Dec. — Vol. 32, no. 6. — P. 3231–3242. — ISSN 2469-9934. — DOI: 10.1103/PhysRevA.32.3231.
- 20 Giant resonances near the split band edges of two-dimensional photonic crystals / H. Noh [et al.] // *Phys. Rev. A.* — 2010. — July. — Vol. 82, no. 1. — P. 013801. — ISSN 2469-9934. — DOI: 10.1103/PhysRevA.82.013801.
- 21 Extremely subradiant states in a periodic one-dimensional atomic array / D. F. Kornovan [et al.] // *Phys. Rev. A.* — 2019. — Dec. — Vol. 100, no. 6. — P. 063832. — ISSN 2469-9934. — DOI: 10.1103/PhysRevA.100.063832.
- 22 *Poddubny A. N.* Quasiflat band enabling subradiant two-photon bound states // *Phys. Rev. A.* — 2020. — Apr. — Vol. 101, no. 4. — P. 043845. — ISSN 2469-9934. — DOI: 10.1103/PhysRevA.101.043845.
- 23 *Quan Q., Loncar M.* Deterministic design of wavelength scale, ultra-high Q photonic crystal nanobeam cavities // *Opt. Express.* — 2011. — Sept. — Vol. 19, no. 19. — P. 18529–18542. — ISSN 1094-4087. — DOI: 10.1364/OE.19.018529.
- 24 *Yariv A., Yeh P.* *Optical Waves in Crystals: Propagation and Control of Laser Radiation.* — Hoboken, NJ, USA : Wiley, 11/2002. — ISBN 978-0-471-43081-0. — URL: <https://www.wiley.com/en-us/Optical+Waves+in+Crystals%3A+Propagation+and+Control+of+Laser+Radiation-p-9780471430810>.
- 25 *Figotin A., Vitebskiy I.* Gigantic transmission band-edge resonance in periodic stacks of anisotropic layers // *Phys. Rev. E.* — 2005. — Sept. — Vol. 72, no. 3. — P. 036619. — ISSN 2470-0053. — DOI: 10.1103/PhysRevE.72.036619.
- 26 *Zhang Y.-X., Mølmer K.* Subradiant Emission from Regular Atomic Arrays: Universal Scaling of Decay Rates from the Generalized Bloch Theorem // *Phys. Rev. Lett.* — 2020. — Dec. — Vol. 125, no. 25. — P. 253601. — ISSN 1079-7114. — DOI: 10.1103/PhysRevLett.125.253601.

- 27 *Figotin A., Vitebskiy I.* Slow wave phenomena in photonic crystals // *Laser Photonics Rev.* — 2011. — Mar. — Vol. 5, no. 2. — P. 201–213. — ISSN 1863-8880. — DOI: 10.1002/lpor.200900049.
- 28 *Burr J. R., Reano R. M.* Zero-coupling-gap degenerate band edge resonators in silicon photonics // *Opt. Express.* — 2015. — Nov. — Vol. 23, no. 24. — P. 30933–30942. — ISSN 1094-4087. — DOI: 10.1364/OE.23.030933.
- 29 Multipole analysis of light scattering by arbitrary-shaped nanoparticles on a plane surface / *A. B. Evlyukhin [et al.]* // *J. Opt. Soc. Am. B, JOSAB.* — 2013. — Oct. — Vol. 30, no. 10. — P. 2589–2598. — ISSN 1520-8540. — DOI: 10.1364/JOSAB.30.002589.
- 30 *Babicheva V. E., Evlyukhin A. B.* Analytical model of resonant electromagnetic dipole-quadrupole coupling in nanoparticle arrays // *Phys. Rev. B.* — 2019. — May. — Vol. 99, no. 19. — P. 195444. — ISSN 2469-9969. — DOI: 10.1103/PhysRevB.99.195444.
- 31 Exponential Improvement in Photon Storage Fidelities Using Subradiance and “Selective Radiance” in Atomic Arrays / *A. Asenjo-Garcia [et al.]* // *Phys. Rev. X.* — 2017. — Aug. — Vol. 7, no. 3. — P. 031024. — ISSN 2160-3308. — DOI: 10.1103/PhysRevX.7.031024.
- 32 Coupled mode theory analysis of mode-splitting in coupled cavity system / *Q. Li [et al.]* // *Opt. Express.* — 2010. — Apr. — Vol. 18, no. 8. — P. 8367–8382. — ISSN 1094-4087. — DOI: 10.1364/OE.18.008367.
- 33 One-Dimensional High-Q Silicon Nanoparticle Chain Resonators for Refractive Index Sensing / *L. Ding [et al.]* // *ACS Appl. Nano Mater.* — 2022. — Mar. — Vol. 5, no. 3. — P. 3170–3176. — DOI: 10.1021/acsanm.1c03866.